



**Calhoun: The NPS Institutional Archive**

---

Theses and Dissertations

Thesis Collection

---

1955

# High energy photo-ejection of neutron-proton pairs from various nuclei.

Wilson, Henry Hamilton

Massachusetts Institute of Technology

---

<http://hdl.handle.net/10945/14245>



Calhoun is a project of the Dudley Knox Library at NPS, furthering the precepts and goals of open government and government transparency. All information contained herein has been approved for release by the NPS Public Affairs Officer.

**Dudley Knox Library / Naval Postgraduate School**  
**411 Dyer Road / 1 University Circle**  
**Monterey, California USA 93943**

<http://www.nps.edu/library>

**HIGH ENERGY PHOTO-EJECTION OF NEUTRON-PROTON  
PAIRS FROM VARIOUS NUCLEI**

---

**Henry Hamilton Wilson**











JF 214

HIGH ENERGY PHOTO-EJECTION OF NEUTRON-PROTON  
PAIRS FROM VARIOUS NUCLEI

by

HENRY HAMILTON WILSON  
B.S., United States Naval Academy  
(1947)

SUBMITTED IN PARTIAL FULFILLMENT OF THE  
REQUIREMENTS FOR THE DEGREE OF  
MASTER OF SCIENCE  
at the  
MASSACHUSETTS INSTITUTE OF TECHNOLOGY  
June, 1955

Signature of Author.....  
Department of Physics, May 23, 1955

Certified by.....  
Thesis Supervisor

Accepted by.....  
Chairman, Departmental Committee on Graduate Students





## ABSTRACT

HIGH ENERGY PHOTO-EJECTION OF NEUTRON-PROTON  
PAIRS FROM VARIOUS NUCLEIby  
HENRY HAMILTON WILSON

Submitted to the Department of Physics on May 23, 1955 in  
partial fulfillment of the requirements for the degree of  
Master of Science

Neutrons have been observed in coincidence with high energy photoprotons in this and other laboratories. For a fixed proton energy and angle the neutrons detected in coincidence with these protons possess an angular distribution about the angle predicted for the ejection of the neutron by the kinematics of a gamma ray interaction with a deuteron at rest. The neutrons in coincidence with photoprotons at angles beyond those expected from the resolution of the detectors can arise from initial nucleon momenta. This suggested that the shape of these neutron angular distributions could be employed as a mode of studying the average momenta and perhaps the momentum distributions of nucleons in different nuclei.

Curves were taken for deuterium, lithium, carbon, oxygen, aluminum and copper. The deuterium curve was taken as an experimental check on the resolution of the equipment. A finite angular spread was noted in lithium beyond that due to the resolution of the detectors. A marked increase in the angular spread occurred between lithium and carbon with a slight further increase for aluminum and copper.

A crude theory has been developed for the shape of these curves. A three-dimensional gaussian distribution is assumed. It was fitted to the lithium data with a  $1/e$  value of approximately 9 Mev and to carbon and oxygen with a  $1/e$  value of approximately 19 Mev. The aluminum and copper do not fit the theoretical shape. The possibility exists that neutrons scattered within the nucleus broaden such curves in these nuclei.

Thesis Supervisor: Bernard T. Feld  
Title: Associate Professor of Physics

28993



## ACKNOWLEDGEMENTS

I am deeply indebted to Dr. Albert Wattenberg and Professor Bernard T. Feld for constant guidance and valuable support in the theoretical aspects of this work. Allen Odian, Peter Stein and Dr. Roy Weinstein ably assisted in the preparation of the equipment and during the measurements. Thanks are also due to William Rankin and Eugene Christie for assistance during the measurements.

This work was in part supported jointly by the Atomic Energy Commission and the Office of Naval Research.



# MEMORANDUM

I am deeply indebted to Mr. J. H. ... and ...  
 ... to the ... of ...  
 ... and Dr. ...  
 ... of the ...  
 ... and ...

This work was ...  
 ...

...

...

...

## TABLE OF CONTENTS

	Page
Abstract.....	2
Acknowledgements.....	3
Index to Drawings.....	6
Index to Tables.....	7
I Introduction.....	8
A. Photo-Nuclear Processes.....	8
B. Momenta of Nucleons in Nuclei.....	11
II Experimental Equipment.....	19
A. Accelerator and Monitor.....	19
B. Counter Telescopes.....	19
C. Electronics.....	24
D. Targets.....	31
III Experimental Procedure.....	35
A. Standards.....	35
B. Treatment of Accidentals.....	35
C. Kinematics.....	36
D. Description of Runs.....	36
IV Analysis of Data.....	38
A. Reduction of Raw Data.....	38
B. Deuterium.....	38
C. Resolution of Equipment.....	46
D. Reliability of the Data.....	48

# TABLE OF CONTENTS

.....	1
.....	2
.....	3
.....	4
.....	5
.....	6
.....	7
.....	8
.....	9
.....	10
.....	11
.....	12
.....	13
.....	14
.....	15
.....	16
.....	17
.....	18
.....	19
.....	20
.....	21
.....	22
.....	23
.....	24
.....	25
.....	26
.....	27
.....	28
.....	29
.....	30
.....	31
.....	32
.....	33
.....	34
.....	35
.....	36
.....	37
.....	38
.....	39
.....	40
.....	41
.....	42
.....	43
.....	44
.....	45
.....	46
.....	47
.....	48
.....	49
.....	50
.....	51
.....	52
.....	53
.....	54
.....	55
.....	56
.....	57
.....	58
.....	59
.....	60
.....	61
.....	62
.....	63
.....	64
.....	65
.....	66
.....	67
.....	68
.....	69
.....	70
.....	71
.....	72
.....	73
.....	74
.....	75
.....	76
.....	77
.....	78
.....	79
.....	80
.....	81
.....	82
.....	83
.....	84
.....	85
.....	86
.....	87
.....	88
.....	89
.....	90
.....	91
.....	92
.....	93
.....	94
.....	95
.....	96
.....	97
.....	98
.....	99
.....	100

	Page
V Results.....	50
A. Deuterium.....	50
B. Lithium.....	50
C. Carbon.....	55
D. Oxygen.....	55
E. Aluminum.....	60
F. Copper.....	60
VI Conclusions.....	65
Bibliography.....	70
Appendix I A Crude Theory of the Cruve Shapes.....	72





## INDEX TO DRAWINGS

Figure	Page
1. General Arrangement of Experimental Equipment.....	20
2. Details of Proton Detector Lucite Frame.....	22
3. Pulse Height versus Proton Energy Curves for Proton..... Telescope Crystals	25
4. Details of Neutron Detector.....	27
5. Electronics Block Diagram.....	29
6. Neutron-Proton Coincidences From Deuterium.....	51
7. Neutron-Proton Coincidences From Lithium.....	53
8. Neutron-Proton Coincidences From Carbon.....	56
9. Neutron-Proton Coincidences From Oxygen.....	58
10. Neutron-Proton Coincidences From Aluminum.....	61
11. Neutron-Proton Coincidences From Copper.....	63
12. Fit of Experimental Data for Lithium, Carbon and..... Oxygen to Theoretical Curve Shape	67

INDEX TO DRAWINGS

Figure	Page
1. General Arrangement of Experimental Apparatus.....	20
2. Details of Proton Detector Inside Frame.....	22
3. Pulse Height versus Proton Energy Curves for Proton..... Talcum Crystals	23
4. Details of Neutron Detector.....	27
5. Illustrative Block Diagram.....	29
6. Neutron-Proton Coincidences from Lithium.....	31
7. Neutron-Proton Coincidences from Lithium.....	33
8. Neutron-Proton Coincidences from Carbon.....	36
9. Neutron-Proton Coincidences from Oxygen.....	38
10. Neutron-Proton Coincidences from Aluminum.....	41
11. Neutron-Proton Coincidences from Copper.....	43
12. Fit of Experimental Data for Lithium, Carbon and..... Oxygen to Theoretical Curves	47

## INDEX TO TABLES

Table	Page
I Summary of Other Investigations of Nucleon Momenta.....	17
II Target Data.....	32
III Sample of Data Recorded During Runs.....	39
IVa Summary of Heavy Water Data.....	40
IVb Summary of Lithium Data.....	41
IVc Summary of Carbon Data.....	42
IVd Summary of Light Water (Oxygen) Data.....	43
IVe Summary of Aluminum Data.....	44
IVf Summary of Copper Data.....	45
V Reduction of Data for Deuterium from $D_2O$ and $H_2O$ .....	47





## I. Introduction

### A. Photo-Nuclear Processes

The production of photoprotons as a result of the reaction of gamma rays with different nuclei has been studied by many investigators<sup>1</sup>. The types of interactions of gamma rays with nuclei by which the photoprotons are produced vary with the energy of the gamma ray<sup>2</sup>. In the region of higher photon energies above approximately 100 Mev the predominant reaction results in an ejected proton which frequently possesses an energy comparable to that of the incident gamma ray. The common method of observing these higher energy reactions has been to bombard the target nuclei with high energy x-rays from bremsstrahlung sources. Because the bremsstrahlung spectrum falls off rapidly with increasing energy the strong weighting of lower energy protons makes interpretation of the observations difficult.

However, numerous observations have resulted in a large amount of information on high energy protons from x-rays on various targets. Protons of energies between 10 and 70 Mev were studied by Levinthal and Silverman<sup>3</sup> using the 322 Mev Berkeley synchrotron yielding a proton energy spectrum which fell off roughly as  $E^{-2}$ . While the 10 Mev protons were ejected isotropically (probably the tail of the evaporation spectra) the 40 Mev protons showed a distinct forward peaking in angular distribution. Walker<sup>4</sup> employed a 195 Mev x-ray beam from the Cornell synchrotron to observe protons of energies greater than about 70 Mev. He observed a forward peaking in the angular distribution and a more rapid decrease with energy of about

## 1. Introduction

## A. Photo-Nuclear Processes

The production of photo-neutrons as a result of the reaction of gamma rays with different nuclei has been studied by many investigators. The types of interactions of gamma rays with nuclei by which the photo-neutrons are produced vary with the energy of the gamma ray. In the region of higher photon energies there are approximately 100 different reactions which result in an ejected neutron which is isotropic in energy comparable to that of the incident gamma ray. The common method of observing these interactions has been to bombard the target nuclei with high energy gamma rays from bremsstrahlung sources. Because the bremsstrahlung spectrum falls off rapidly with increasing energy the strong weighting at lower energy prevents exact interpretation of the observations.

However, neutron observations have resulted in a large amount of information on high energy neutron from gamma ray various targets. Protons of energies between 10 and 20 MeV were ejected by Leventhal and Silverman<sup>2</sup> using the 325 MeV Berkeley synchrotron yielding a proton energy spectrum which fell off roughly as  $E^{-2}$ . While the 10 MeV protons were ejected isotropically (probably the tail of the evaporation spectra) the 40 MeV protons showed a distinct forward peaking in angular distribution. Silverman employed a 195 MeV x-ray beam from the Cornell synchrotron to observe protons of energies greater than about 70 MeV. He observed a forward peaking in the angular distribution and a very rapid decrease with energy of about



$E^{-5}$  in the integral proton spectra. Observations of protons up to energies of about 200 Mev and over wider ranges of angles and target elements were made by Keck<sup>5</sup> at Cornell using 300 Mev x-rays. He observed the following: the cross section for photoproton ejection increased linearly with atomic number; the angular distributions peaked more in the forward direction with increasing energy; and the proton spectra showed a sharp break in slope at an energy of approximately half of the maximum photon energy.

Levinger<sup>6</sup>, on the basis of the last feature, developed theoretically a model in which the energetic photoprotons result from the direct interaction of the photons with neutron-proton pairs (i.e. deuteron like sub units) in the nucleus. Further confirmation for Levinger's model came from the measurements of Rosengren and Dudley<sup>7</sup> using 322 Mev x-rays from the Berkeley synchrotron, by Perry and Keck<sup>8</sup> who employed a subtraction technique to obtain the effect of monochromatic gamma rays, by Weil and McDaniel<sup>9</sup> using monochromatic 190 Mev gamma rays and by Feld et al<sup>2</sup> in this laboratory.

However, other features of the high energy photo-production distributions are not nearly as successfully accounted for by the quasi-deuteron model of Levinger<sup>6</sup>. In particular, the observed angular distributions appeared to be more strongly peaked in the forward direction than those predicted by the model.

Feld et al<sup>2</sup> observed the angular distribution of protons of 126, 169 and 203 Mev. The results differed from the predictions of Levinger's model in the positions of the maxima (if any) and the failure to observe a kinematical "cutoff". The quasi-deuteron model



$\gamma$  in the total proton spectrum. Observation of protons up to  
 energies of about 300 Mev and over wider ranges of angles and larger  
 elements were made by Kock<sup>2</sup> at Cornell using 300 Mev x-rays. He  
 observed the following: the cross section for absorption of protons  
 increased linearly with atomic number; the angular distribution  
 peaked more in the forward direction with increasing energy; and the  
 proton spectra showed a sharp break in slope at an energy of  
 approximately half of the maximum photon energy.  
 Livingston<sup>3</sup>, on the basis of the last feature, developed  
 theoretically a model in which the energetic photo-neutrons result  
 from the direct interaction of the photon with neutron-proton  
 pairs (i.e., between 1.01 and 1.02 Mev) in the nucleus. Further confir-  
 mation for Livingston's model came from the measurements of Livingston  
 and Gellert<sup>4</sup> using 322 Mev x-rays from the Berkeley synchrotron, by  
 Kock and Kock<sup>5</sup> who employed a subtraction technique to obtain the  
 effect of nonionizing gamma rays, by Bell and Michael<sup>6</sup> using  
 monochromatic 130 Mev gamma rays and by Bell et al.<sup>7</sup> in this laboratory.  
 However, other features of the high energy photo-production  
 distributions are not nearly so successfully accounted for by the  
 quasi-free model of Livingston<sup>3</sup>. In particular, the observed angular  
 distributions appeared to be more strongly peaked in the forward  
 direction than those predicted by the model.  
 Bell et al.<sup>7</sup> observed the angular distribution of protons at  
 120, 160 and 203 Mev. The results differed from the prediction of  
 Livingston's model in the position of the minima (17 deg) and the  
 failure to observe a kinematical "cutoff". The quasi-free model

would predict pronounced maxima between 30 and 60 degrees for the energies at which the observations were made. According to Feld et al.<sup>2</sup> the peaks (if any) were well below 30 degrees. It was pointed out by Rosengren and Dudley<sup>7</sup> that this does not necessarily contradict the quasi-deuteron model as Levinger assumed a  $\sin^2\theta$  angular distribution in the center of mass system for the deuteron photodisintegration. A flatter, or forward peaked deuteron cross section (which is not excluded by the existing data on the photodisintegration of the deuteron<sup>10,11</sup>), would be consistent with the observed high energy photoproton distributions from heavier nuclei.

The failure to observe a kinematical "cutoff" in the angular distribution can be reconciled with the quasi-deuteron model if the distributions of the nucleons within a carbon nucleus contain a very large component of nucleons with relatively higher momenta than that predicted by the Fermi distribution.

A more direct test of the quasi-deuteron model is the observance of the simultaneous emission of a neutron and a proton together with their angular correlations. Such events have been observed by Myers, Odian, Stein and Wattenberg<sup>12</sup> in this laboratory and by Barton and Smith<sup>13</sup> employing 265 Mev bremsstrahlung from the University of Illinois betatron. Substantial support for the quasi-deuteron model was provided by these observations. The neutron-proton coincidences were observed to have the kinematical relationships of a deuteron in motion\*.

\*For a discussion of  $\theta$  and curves relating to the kinematics of the photodisintegration of the deuteron see Wiener<sup>14</sup> who used relativistic momentum and energy conservation to calculate the energy and angular distributions.



would predict a pronounced maximum between 30 and 40 degrees for low energies at which the cross-sections were small. According to field of the peaks (if any) were well below 30 degrees. It was pointed out by Rosenzweig and Bellamy that this does not necessarily contradict the quasi-deuteron model as having associated a  $\frac{1}{2}$  spin angular distribution in the center of mass system for the deuteron phase distribution. A flatter, or indeed peaked distribution cross section (which is not included by the existing data on the photodisintegration of the deuteron  $^{10,11}$ ), would be consistent with the observed high energy photoproton distribution from heavier nuclei.

The failure to observe a kinematical "corner" in the angular distribution can be reconciled with the quasi-deuteron model if the distribution of the nucleons within a carbon nucleus consists of two large components of nucleons with relatively higher momenta than those predicted by the Fermi distribution.

A more direct test of the quasi-deuteron model is the observation of the simultaneous emission of a neutron and a proton together with their angular correlation. Such events have been observed by O'Brien, O'Brien and Wetherby<sup>12</sup> in this laboratory and by Rosenzweig and Bellamy<sup>13</sup> at the University of Illinois.

Substantial support for the quasi-deuteron model was provided by these observations. The neutron-proton angular distribution was observed to have the kinematical characteristics of a deuteron in motion.

over a distribution of and curves relating to the kinematics of the photodisintegration of the deuteron are shown in the next section. The energy conservation is calculated to calculate the energy and angular distributions.

The results obtained showed a broader angular distribution (for fixed proton energy and angle) of neutrons about the predicted angles for heavier nuclei than for deuterium. It is manifest that this angular distribution can arise from the momenta of the nucleons within the nucleus.

Studies by Wattenberg et al (unpublished) were made in this laboratory of the widths of the neutron angular distribution as a function of energy of the photoprotons (and therefore of the photo-neutron). These studies showed that the widths could be quantitatively connected with the internal momentum of the quasi-deuteron. The possibility arose of employing this effect as a tool to study the momenta of nucleons within a nucleus. In this connection a discussion of previous information on the momenta of nucleons within a nucleus is in order.

#### B. Momenta of Nucleons in Nuclei

Nuclear internal momenta have been studied by several observers employing different techniques; also the application of several proposed theoretical momentum distributions to experimental results has been attempted. Among the proposed momentum distributions are the statistical gas model of Fermi<sup>15</sup>, the Chew-Goldberger<sup>16</sup> distribution and the gaussian distribution.

Fermi<sup>15</sup> employed a statistical gas model of the nucleus. The nucleus is considered to be a gas of neutrons and protons confined to a volume  $\Omega = \frac{4}{3}\pi R_0^3 A$ .

The number of states of



The results obtained showed a broader angular distribution (for fixed position energy and angle) of neutrons about the parallel angles for heavier nuclei than for deuterium. It is evident that this angular distribution can arise from the emission of the neutrons within the nucleus.

Studies by G. S. Gurevich et al. (unpublished) were made in this laboratory of the widths of the neutron angular distribution as a function of energy of the deuterons (and thickness of the proton neutron). These studies showed that the widths could be quantitatively connected with the internal structure of the deuteron. The possibility arose of applying this effect as a tool to study the structure of nuclei as well as neutrons. In this connection a discussion of previous information on the structure of nuclei at this energy is in order.

## 2. Structure of Nuclei at High Energies

Nuclear internal structure have been studied by several observers employing different techniques; also the collection of several proposed theoretical neutron distribution to experimental results has been attempted. Among the proposed neutron distribution are the statistical gas model of Fermi<sup>1,2</sup>, the shell-theory distribution<sup>3</sup> and the liquid drop model.

Fermi<sup>1,2</sup> employed a statistical gas model of the nucleus. The nucleus is considered to be a gas of neutrons and protons confined to a volume  $\Omega = \frac{4}{3}\pi R_0^3 A$ . The number of states of

momentum,  $n$ , less than  $P_{\max}$  of a proton confined to  $\Omega$  is

$$n = 2 \frac{4\pi P_{\max}^3 \Omega}{3(2\pi\hbar)^3} \quad (\text{factor 2 is for spin})$$

If the degeneracy is complete,  $n = Z$ ; hence:

$$P_{\max}^{\text{proton}} = (3\pi^2)^{\frac{1}{3}} \hbar \left(\frac{Z}{\Omega}\right)^{\frac{1}{3}}$$

and  $N = A - Z$  for the neutrons

$$P_{\max}^{\text{neutron}} = (3\pi^2)^{\frac{1}{3}} \hbar \left(\frac{A-Z}{\Omega}\right)^{\frac{1}{3}}$$

Making the approximation that  $Z = N = \frac{A}{2} = n$

$$P_{\max} = (3\pi^2)^{\frac{1}{3}} \left( \frac{A}{2 \frac{4\pi}{3} R_0^3 A} \right)^{\frac{1}{3}}$$

This corresponds to kinetic energies in the range from 21 to 29 Mev depending on the value of  $R_0$  employed<sup>17</sup>. This formulation predicts that all momentum states are occupied up to this maximum and none above it.

To fit the results of observations by Hadley and York<sup>18</sup>, Chew and Goldberger<sup>16</sup> postulated a momentum distribution for carbon:

$$\frac{\alpha}{\pi^2(\alpha^2 + p^2)}$$

where  $\alpha$  is a momentum corresponding to a nucleon energy of 18 Mev.

The gaussian distribution is proportional to  $e^{-\frac{p^2}{2mE_g}}$

The gaussian is the same in both momentum and  $x$  space.

The usual and most obvious approach to the study of nuclear internal momenta is by observation of an interaction with a single nucleon in the nucleus. Results of these interactions are analyzed on a kinematic basis and the energy and/or angular spreads obtained are ascribed to the initial momentum of the nucleons within the nucleus. Also the deviations in threshold energies for  $\pi$  meson production has



normalization, we have that  $\int_{-\infty}^{\infty} \rho(x) dx = 1$ .

$$n = \frac{1}{2} \frac{4\pi p_{max}^2}{(2\pi)^3} \frac{1}{A} \int_{-\infty}^{\infty} \rho(x) dx$$

If the distribution is isotropic,  $n = \frac{1}{2} \frac{4\pi p_{max}^2}{(2\pi)^3} \frac{1}{A} \int_{-\infty}^{\infty} \rho(x) dx$ .

$$p_{max} = (3\pi^2)^{\frac{1}{3}} n^{\frac{1}{3}} \left( \frac{A}{2\pi} \right)^{\frac{1}{3}}$$

and  $n = \frac{1}{2} \frac{4\pi p_{max}^2}{(2\pi)^3} \frac{1}{A} \int_{-\infty}^{\infty} \rho(x) dx$  for the isotropic case.

$$p_{max} = (3\pi^2)^{\frac{1}{3}} n^{\frac{1}{3}} \left( \frac{A}{2\pi} \right)^{\frac{1}{3}}$$

Using the approximation that  $n = \frac{1}{2} \frac{4\pi p_{max}^2}{(2\pi)^3} \frac{1}{A} \int_{-\infty}^{\infty} \rho(x) dx$ .

$$p_{max} = (3\pi^2)^{\frac{1}{3}} n^{\frac{1}{3}} \left( \frac{A}{2\pi} \right)^{\frac{1}{3}}$$

This corresponds to kinetic energies in the range from 11 to 13 MeV.

depending on the value of  $\rho_0$  employed. The normalization procedure

that all momentum states are occupied up to this maximum and none

above it.

To fit the results of observations by Healey and Tarr, 1967.

They and Goldberger 1967 assumed a momentum distribution for neutrons

$$\frac{1}{(2\pi)^3} \frac{1}{\alpha^2 + q^2}$$

where  $\alpha$  is a constant corresponding to a nuclear energy of 11 MeV.

The Gaussian distribution is proportional to  $e^{-\frac{q^2}{2m\alpha^2}}$ .

The function is the same in both momentum and  $q$  space.

The small and most obvious approach to the study of nuclear

internal structure is by observation of an interaction with a single

nucleon in the nucleus. Results of these interactions are analyzed

on a kinematic basis and the energy and/or angular momenta obtained

are assigned to the initial momentum of the nucleon within the nucleus.

Also the deviations in threshold energies for  $\pi$  meson production has

been employed to provide information on nucleon momenta.

Hadley and York<sup>18</sup> employed a beam of 90 Mev neutrons from the 184-in. Berkeley synchrocyclotron to produce deuterons from the bombardment of target nuclei. In this case the neutron "picks up" a partner proton from the nucleus and emerges as a deuteron. Since it is necessary for the relative momenta of the proton and the neutron to form a state of the deuteron, the process involves the momentum distribution of both the picked up proton and the deuteron. The observed distribution of deuterons for carbon was explained somewhat arbitrarily by Chew and Goldberger<sup>16</sup>. However, Heidman<sup>19</sup> was also able to fit an excited Fermi gas distribution, with a temperature corresponding to an excitation of 9 Mev, to York's data.

High energy proton-proton scattering experiments have been performed by Chamberlain and Segrè<sup>20</sup>, Cladis<sup>21</sup> and Wilcox<sup>22</sup> using 340 Mev protons from the Berkeley 184-in. synchrocyclotron. If the struck proton is assumed to be at rest the nonrelativistic energy of the observed proton is  $E_0 \cos^2\theta$  (neglecting the binding energy of the proton and the excitation energy of the residual nucleus) on the basis of the two-body problem where  $E_0$  is the energy of the incident proton and  $\theta$  is the angle of observation. However, the energy spectrum is smeared out due to the finite momentum of the struck proton. Chamberlain and Segrè<sup>20</sup> studied pairs of protons emitted in coincidence from lithium as a function of the angle between the two protons. The resulting data could be fitted with a Fermi gas momentum distribution with a maximum energy of 20 Mev.



been employed to provide information on neutron spectra.

Valley and York<sup>12</sup> employed a beam of 30 keV neutrons from the Illinois Wesleyan synchrotron to produce neutrons from the bombardment of targets needed. In this case the neutron yields are a factor of 100 from the analysis and appear as a constant. There is a necessity for the relative number of the protons and the neutrons in the beam of the detector, the process involves the constant distribution of both the labeled and unlabeled protons. The observed distribution of neutrons for carbon was calculated assuming approximately by Chen and Goldberger<sup>13</sup>. However, Goldberger<sup>14</sup> was also able to fit an excited state distribution with a temperature corresponding to an excitation of 9 MeV to 10 MeV data.

High energy proton-proton scattering experiments have been performed by Chamberlain and Feghly<sup>15</sup>, Glashow<sup>16</sup> and Wilson<sup>17</sup> using 340 MeV protons from the Berkeley 184-in. synchrotron. If the kinetic energy is assumed to be as high as the kinetic energy of the observed proton is  $E_p$  (neglecting the kinetic energy of the proton and the rest mass energy of the residual nucleus) in the rest of the two-body proton state  $E_0$  is the energy of the incident proton and  $\theta$  is the angle of observation. However, the energy spectrum is measured out due to the finite number of the observed protons. Chamberlain and Feghly<sup>15</sup> studied pairs of protons which in addition to the kinetic energy of the proton between the two protons. The resulting data could be fitted with a level free momentum distribution with a maximum energy of 30 MeV.

Cladis<sup>21</sup> observed the distribution of single protons quasi-elastically scattered from carbon at 40 degrees. The nuclear internal momentum he deduced was best fitted by a Gaussian distribution with a  $1/e$  value of about 16 Mev.

Wilcox<sup>22</sup> studied by proton-proton coincidences the momentum of the protons emerging from the collisions. He observed coincidences from hydrogen, deuterium, beryllium, lithium and boron. He found the best fit to the experimental data for beryllium was a gaussian momentum distribution with a  $1/e$  value of 20 Mev. However, any value between 15 and 25 Mev would fit the data. Fermi (rectangular) and Chew-Goldberger distributions did not fit as well. An excited Fermi distribution would fit within the accuracy of the experiment. He observed qualitative differences between lithium, beryllium and boron. He interpreted these on the basis of the proton distribution in the nucleus.

The shift in the threshold for meson production from free nucleon-nucleon production to nucleon-nucleus production has been used to examine nuclear internal momenta. The threshold energy required in the nucleon-nucleus reaction is lower than that required by the free nucleon-nucleon reaction by the energy corresponding to the momentum of the nucleon in the nucleus as predicted by McMillan and Teller<sup>23</sup>. Henley and Huddleston<sup>24</sup> and Henley<sup>25</sup> have discussed the nucleonic production of  $\pi$  mesons in complex nuclei using several momentum distributions. The distribution employed affects the production threshold, excitation function and the energy spectrum and angular distribution of the produced mesons as compared with those resulting from collisions with



directly observed the distribution of angles between nuclei-  
 elastically scattered from carbon at 10 degrees. The nuclear angular  
 distribution he obtained was best fitted by a Gaussian distribution with a  
 1/2 value of about 10 deg.

Wilson<sup>22</sup> studied by proton-proton collisions the angular dis-  
 tribution resulting from the collision. He observed coincidences  
 from hydrogen, deuterium, tritium, helium and carbon. He found the  
 best fit in the experimental data for tritium was a Gaussian distribution  
 distribution with a 1/2 value of 20 deg. However, very little deviation  
 is and 25 deg would fit the data. Tani (1954) and Gross (1954) gave  
 distributions did not fit as well. An earlier found distribution would  
 fit with the accuracy of the experiment. He observed relative  
 differences between tritium, helium and carbon. He interpreted these  
 as the basis of the proton distribution in the nucleus.

The data in the threshold for many reactions from two  
 neutron-neutron reactions to neutron-neutron reactions has been used  
 to measure nuclear angular momentum. The first-order energy levels in  
 the nucleus-nucleus reaction is lower than what is expected by the two  
 neutron-neutron reaction by the energy corresponding to the momentum of  
 the nucleus in the nucleus as predicted by Wilson and Wilson<sup>23</sup>. Wilson  
 and Wilson<sup>24</sup> have discussed the nuclear production  
 of a nucleus in complex nuclei and several nuclear distributions.  
 The distribution employed differs the production threshold, scattering  
 function and the energy spectrum and angular distribution of the  
 produced nucleus as compared with those resulting from collisions with

free nucleons used as targets. Henley found that a gaussian distribution with a  $1/e$  value of 19.3 Mev was the best fit to the data. He also used a 0°K Fermi degenerate gas model distribution and a modified Chew-Goldberger distribution. To eliminate the excess high momentum components and the infinite average energy in the Chew-Goldberger distribution he suggested the following modified form:

$$\frac{1}{(\alpha^2 + p^2)^2 (\beta^2 + p^2)^2}$$

where  $B = 2.5 \alpha$ . This has an average energy of 48.1 Mev and yet fits York's data fairly well. Block, Passman and Havens<sup>26</sup> have performed similar calculations for data obtained at the Columbia cyclotron with an energy of 380 Mev, at first finding the best fit given with the original Chew-Goldberger distribution, but later<sup>27</sup> they have used a gaussian distribution with a  $1/e$  value of 14 Mev.

Bjorklund, Crandall, Moyer and York<sup>28</sup> observed high energy gamma rays resulting from the bombardment of beryllium and carbon with 340 Mev protons from the Berkeley synchrocyclotron in looking for evidence of the  $\pi^0$  meson. They obtained a fit to the results on the assumption that the center of mass system was moving with  $\beta = 0.32$ . If the nucleon had been at rest  $\beta$  would have been 0.39. Because the excitation function increases with energy most of the  $\pi^+$  production comes from nucleons in the target which are moving toward the beam. For  $\beta = 0.32$  the energy of such a proton would be 22 Mev.

Steinberger and Bishop<sup>29</sup> observed the production of mesons from complex nuclei by use of the Berkeley synchrotron bremsstrahlung



These authors used a logarithmic function for the distribution of the number of particles. We also used a logarithmic function for the distribution of the number of particles. It is obvious that the use of a logarithmic function for the distribution of the number of particles is not very accurate. The authors also used a logarithmic function for the distribution of the number of particles. It is obvious that the use of a logarithmic function for the distribution of the number of particles is not very accurate.

$$\frac{1}{(a^2 + b^2)^{\frac{1}{2}} (c^2 + d^2)^{\frac{1}{2}}}$$

where  $a = 2.5 \times 10^{-10}$  cm. This has an average energy of 40.1 eV and yet 10% of the particles have a higher energy. The authors also used a logarithmic function for the distribution of the number of particles. It is obvious that the use of a logarithmic function for the distribution of the number of particles is not very accurate. The authors also used a logarithmic function for the distribution of the number of particles. It is obvious that the use of a logarithmic function for the distribution of the number of particles is not very accurate.

It is obvious that the use of a logarithmic function for the distribution of the number of particles is not very accurate. The authors also used a logarithmic function for the distribution of the number of particles. It is obvious that the use of a logarithmic function for the distribution of the number of particles is not very accurate. The authors also used a logarithmic function for the distribution of the number of particles. It is obvious that the use of a logarithmic function for the distribution of the number of particles is not very accurate.

It is obvious that the use of a logarithmic function for the distribution of the number of particles is not very accurate. The authors also used a logarithmic function for the distribution of the number of particles. It is obvious that the use of a logarithmic function for the distribution of the number of particles is not very accurate.

spectrum. The meson energy and direction of production are broadened from that predicted (by a Comptonlike process) because of the bremsstrahlung spectrum and internal momentum distributions. Lax and Feshback<sup>30</sup> interpreted their results and found agreement with the Chew-Goldberger distribution.

It should be pointed out that it is difficult within the errors of an experiment to say which momentum distribution really fits best, and even when the type of distribution is decided upon its constants are equally difficult to determine (e.g. Wilcox<sup>22</sup>, while he chooses 20 Mev for the  $1/e$  value of the gaussian momentum distribution of beryllium, he finds any value from 15 to 25 Mev a satisfactory fit to the data). Table I contains a brief summary of investigations devoted primarily to nuclear internal momenta. The last column lists the distributions fitted (if any) to their results.

It is to be noted that the previous experimenters (except Wilcox<sup>22</sup>) have studied momentum distributions in a single nucleus. From the above work it appeared worthwhile as a first experiment to investigate whether or not nucleon momenta are the same in different nuclei. From the work of others it appears more difficult to obtain reliable detailed momentum distributions, and there is essentially no information on whether the momentum distributions obtained were specific to the element being studied.

This thesis describes the use of the quasi-deuteron for an experimental study of relative internal momenta. As such the experimental techniques and observations are refinements and extensions to more angles



question, the mean energy and direction of production are determined  
 from data provided (by a Geiger-Müller counter) because of the  
 broadening spectrum and internal momentum distribution. The two  
 methods<sup>23</sup> interpreted their results and found agreement with the  
 Geiger-Müller counter distribution.  
 It should be pointed out that it is difficult within the  
 error of an experiment to say which momentum distribution really fits  
 best, and even when the type of distribution is decided upon the  
 constants are equally difficult to determine (e.g., Wilson<sup>24</sup>, who  
 has chosen 20 Mev for the  $\lambda$  value of the Gaussian momentum distribution  
 of positrons, he finds any value from 15 to 25 Mev is satisfactory fit  
 to the data). Table I contains a brief summary of investigations devoted  
 primarily to nuclear internal momenta. The last column lists the  
 distributions fitted (if any) to their results.  
 It is to be noted that the previous experiments (except  
 Wilson<sup>25</sup>) have studied momentum distributions in a single nucleus.  
 From the above work it appeared worthwhile as a first experiment to  
 investigate whether or not nuclear momenta are the same in different  
 nuclei. From the work of others it appears some difficulty in obtaining  
 reliable detailed momentum distributions, and there is accordingly no  
 information on whether the momentum distributions obtained were specific  
 to the element being studied.  
 This thesis describes the use of the Geiger-Müller counter for an ex-  
 perimental study of relative internal momenta. As with the experimental  
 technique and observations the refinements and extensions to more nuclei

TABLE I

## Summary of Other Investigations of Nucleon Momenta

Author and Reference	Technique	Element	Distribution Applied
Hadley and York <sup>18</sup>	Proton-pickup by neutrons	C	Normal Chew-Goldberger <sup>16</sup>
Chamberlain and Segrè <sup>20</sup>	Angle between protons in P-P scattering	Li	Fermi <sup>15</sup> distribution with maximum energy of 20 Mev
Cladis <sup>21</sup>	"Quasi-elastic" P-P scattering	C	Gaussian with 1/e value of 16 Mev
Wilcox <sup>22</sup>	Momentum analysis of one of the protons from P-P scattering coincidences	Li	None
		Be	Gaussian with 1/e value of 20 Mev
		B	None



TABLE I

Summary of Other Investigations of Nuclear Reactions

Investigator	Reaction	Element	Observations
Bohr and Jensen	Proton-proton by neutrons	0	Neutron energy 1.5 Mev
Bohr and Jensen	Alpha between neutrons in 5-7 MeV	1.5	Neutron energy 50 MeV
Bohr and Jensen	"Alpha-alpha" 5-7 MeV	2	Neutron energy 1.5 MeV
Bohr and Jensen	Neutron alpha of one of the protons from 5-7 MeV	1.5	Neutron energy 1.5 MeV
Bohr and Jensen	Neutron alpha of one of the protons from 5-7 MeV	2	Neutron energy 1.5 MeV

### II. Experimental Equipment

and more nuclei of the previous works in this laboratory<sup>2,12</sup>. As a part of this work it has been necessary to understand the efficiency and angular resolution of the neutron detector employed. This phase of the work has been described separately by Christie<sup>31</sup>.

For the purpose of this work, the neutron detector was a scintillation counter of the type described by Christie<sup>31</sup>. The detector was a 100% efficient detector of the type described by Christie<sup>31</sup>.

The neutron detector was of the liquid scintillator type, for a description of the calibration of this detector see Christie<sup>31</sup> and Hall<sup>32</sup>. The size of nucleus of the detector was reduced to an amount of about  $10^{-10}$  cm. In this experiment the detector corresponded to about  $0.8 \times 10^8$  equivalent nuclei. The number of equivalent nuclei is the total energy in a solid state divided by the nucleus energy.

The general arrangement of the experimental equipment is shown in Figure 1. The various components are described below.

### 5. Scintillation Counter

The method of neutron detection employed was of essentially the same type employed in previous investigations in this laboratory<sup>2</sup>. A thin crystal scintillation counter was employed to detect a fairly homogeneous group of neutrons and to distinguish them from other charged particles by means of pulse height observation. The crystals employed were of Pile 10 plastic. The front crystal was 1 inch thick and the back crystal was 2 inches thick. Both crystals were 1/2 inch in diameter and were mounted in a holder as shown in Figure 2.





## II. Experimental Equipment

### A. Accelerator and Monitor

This experiment was performed with a 340 Mev bremsstrahlung beam from the M.I.T. synchrotron. The synchrotron has a repetition rate of six pulses per second. During each pulse the beam has a duration of about 1200 microseconds.

The monitor employed was of the ionization chamber type. For a description of the calibration of this monitor see Odian<sup>32</sup> and Ratz<sup>33</sup>. The unit of measure of the monitor was referred to as a "mouse". In this experiment the "mouse" corresponded to about  $0.6 \times 10^8$  "equivalent quanta". The number of "equivalent quanta" is the total energy in a photon beam divided by the maximum photon energy.

The general arrangement of the experimental equipment is shown in Figure 1. The various components are described below.

### B. Counter Telescopes

The method of proton detection employed was of essentially the same type employed in previous investigations in this laboratory<sup>2</sup>. A two crystal scintillation counter was employed to detect a fairly monoenergetic group of protons and to distinguish them from other charged particles by means of pulse height observation. The crystals employed were of Pilot "B" plastic. The front crystal was  $\frac{1}{2}$  inch thick and the back crystal was 2 inches thick. Both crystals were 5 inches in diameter and were mounted in a Lucite frame as shown in Figure 2.



## II. Experimental Equipment

### A. Accelerator and Monitor

This experiment was conducted with a Van de Graaff accelerator from the M.I.T. Physics Department. The accelerator has a typical rate of 100 pulses per second. During each pulse the beam has a duration of about 1000 microseconds. The monitor employed one of the ionization chamber type. For a description of the calibration of this monitor see Table 1 and Table 2. The unit of measure of the monitor was referred to as a "count". In this experiment the "counts" corresponded to about  $0.6 \times 10^8$  "equivalent quanta". The number of "equivalent quanta" is the total energy in a beam pulse divided by the average photon energy.

The general arrangement of the experimental equipment is shown in Figure 1. The various components are described below.

### B. Counter Techniques

The method of proton detection employed was of essentially the same type employed in previous investigations in this laboratory.<sup>8</sup> A low crystal scintillation counter was employed to detect a fairly nonconvergent group of protons and to distinguish them from other charged particles by means of pulse height observation. The crystals employed were of PVT "B" plastic. The front crystal was  $\frac{1}{2}$  inch thick and the back crystal was  $\frac{1}{2}$  inch thick. Both crystals were 2 inches in diameter and were mounted in a holder frame as shown in Figure 2.

Figure 1

General Arrangement of Experimental Equipment  
(not to scale)



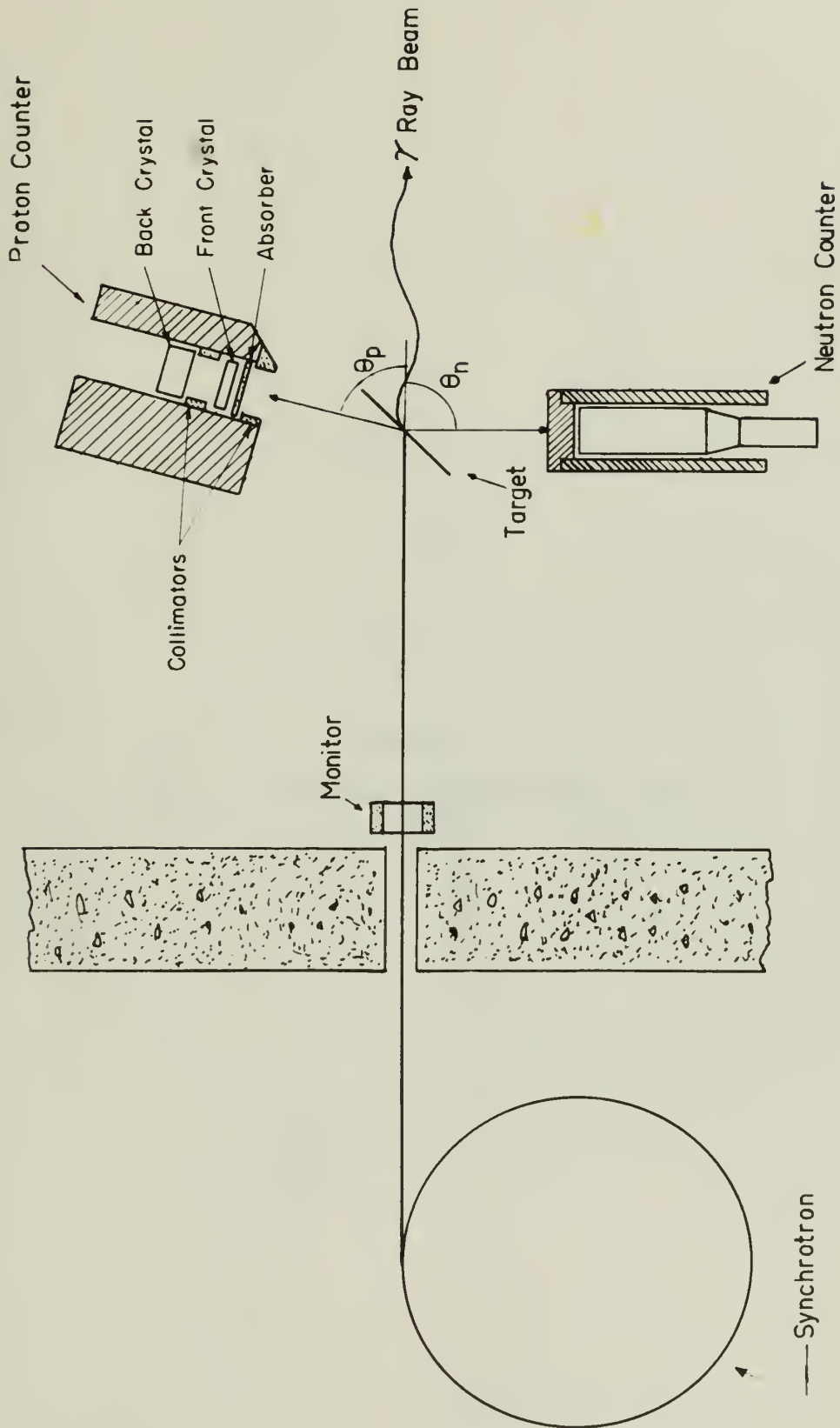


Figure 1





Figure 2

Details of Proton Detector Lucite Frame

Figure 2  
Details of Proton Detector Lucite Frame

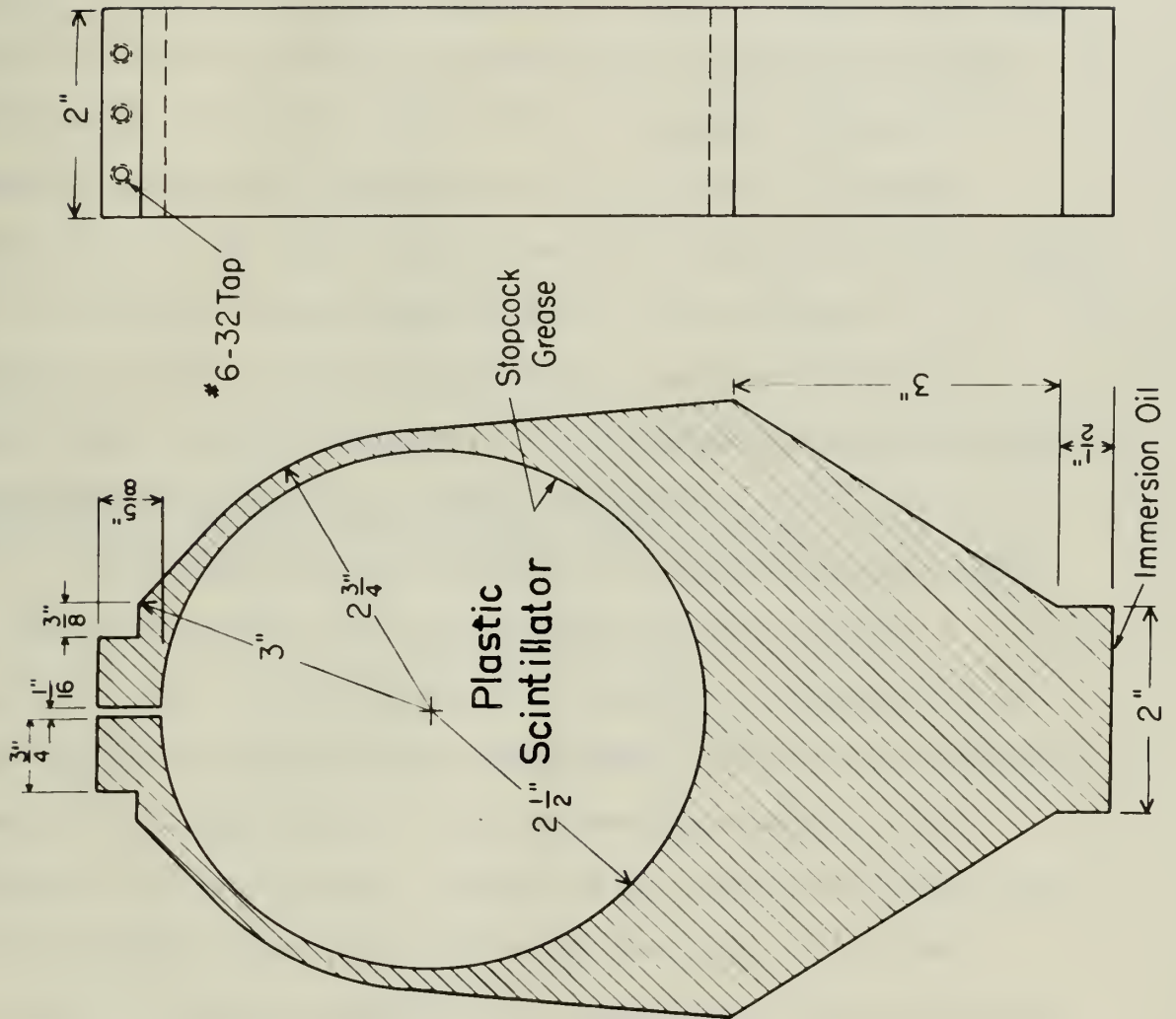


Figure 2





End window (5819) photomultipliers were placed in optical contact with the Lucite frame at a distance of 4 inches from the crystal edge in order to increase the uniformity of the light collection from the crystal. A 0.375 inch brass absorber was placed in front of the front crystal in order to obtain the proper energy group and pulse height relationship in the back crystal. This arrangement corresponded to observing protons with energies from 117 to 142 Mev. Two brass collimators of four inches diameter were also inserted in the telescope. The arrangement of these components may be seen in Figure 1. The energies observed correspond to the peak of the back crystal pulse height curve as shown in Figure 3. For a complete description of the calibration of  $\Delta E$  for this counter see Odian<sup>32</sup>.

The neutron counter consisted of an annealed Lucite cylinder four inches in diameter and 12 inches long as shown in Figure 4. It was filled with a scintillating liquid composed of cyclohexylbenzene with 30 grams of p-terphenyl per liter added. A 5819 photomultiplier tube viewed it from the rear. The side was surrounded by a lead cylinder 1-1/8 inches thick. The face of the counter was behind a two inch lead disk to reduce the entrance of gamma rays and charged particles. A complete description and evaluation of this counter has been furnished by Christie<sup>31</sup>.

### C. Electronics

A block diagram of the electronics is shown in Figure 5. Four amplifier channels were employed. Discriminators and attenuators were

End window (2219) photomultiplier were placed in optical contact with the Lucite frame at a distance of 4 inches from the crystal edge in order to increase the uniformity of the light collection from the crystal. A 0.375 inch brass absorber was placed in front of the front crystal in order to obtain the proper energy group and pulse height relationship in the back crystal. This arrangement corresponded to observing protons with energies from 117 to 142 Mev. Two brass collimators of four inches diameter were also inserted in the collimator. The arrangement of these components may be seen in Figure 1. The energies observed correspond to the peak of the back crystal pulse height curve as shown in Figure 3. For a complete description of the calibration of  $\Delta E$  for this counter see O'Brien<sup>25</sup>.

The neutron counter consisted of an annealed Lucite cylinder four inches in diameter and 12 inches long as shown in Figure 4. It was filled with a scintillating liquid composed of cyclohexylbenzene with 30 grams of p-terphenyl per liter added. A 2119 photomultiplier tube viewed it from the rear. The side was surrounded by a lead cylinder 1-1/8 inches thick. The face of the counter was behind a two inch lead disk to reduce the entrance of gamma rays and charged particles. A complete description and evaluation of this counter has been furnished by Christie<sup>21</sup>.

### C. Electronics

A block diagram of the electronics is shown in Figure 5. Four amplifier channels were employed. Discriminators and coincidence were



## Figure 3

Pulse Height versus Proton Energy Curves for Proton Telescope Crystals

The protons detected corresponded to pulse heights on the back (second) counter above the bias level indicated. Third counter was not used in this experiment.

The positive directed component is quite reliable on the weak (second) counter above the bias level indicated. Third counter was not used in this experiment.

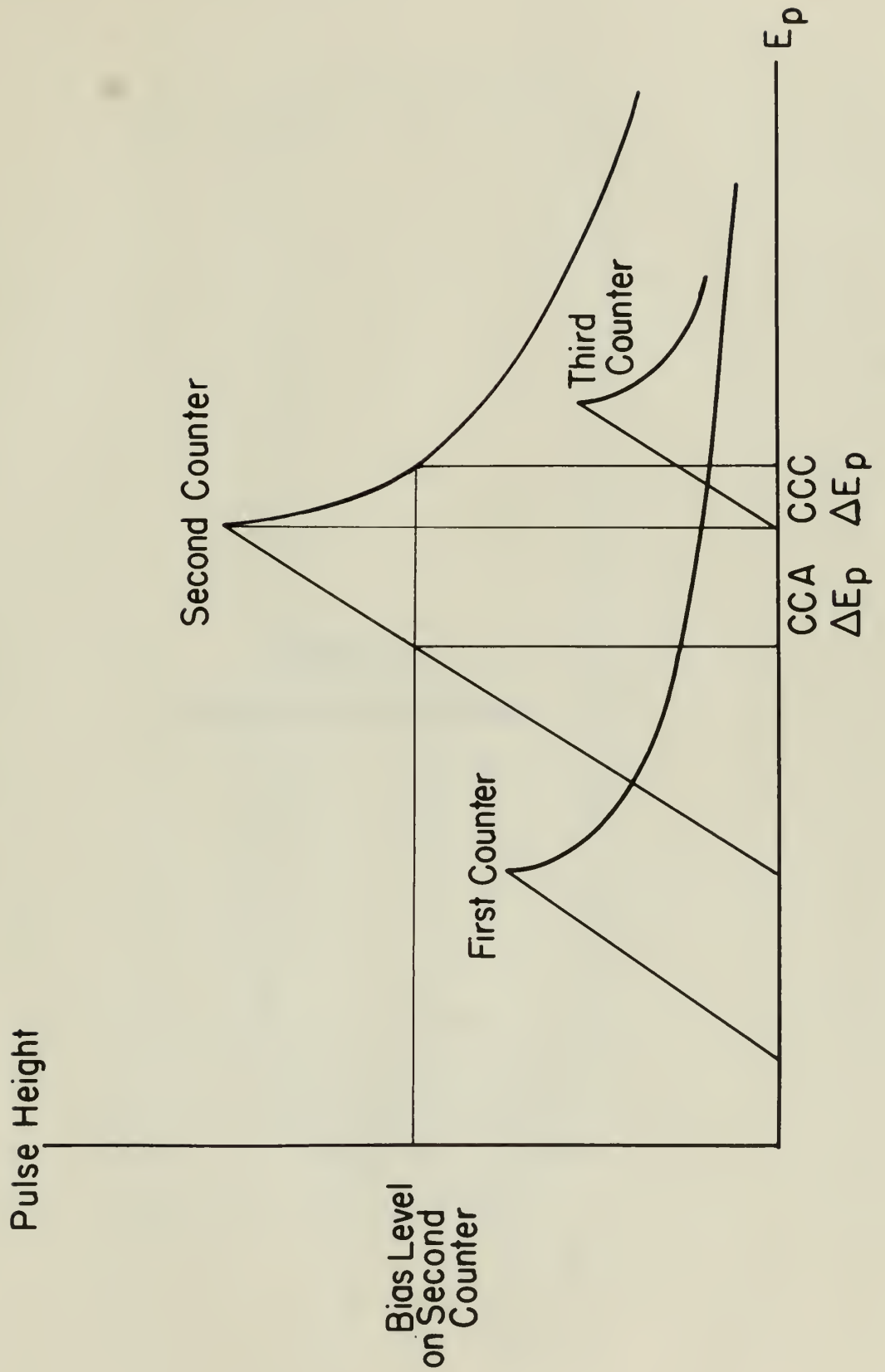


Figure 3





Figure 4  
Details of Neutron Detector

Figure 1  
Outline of Newton's method



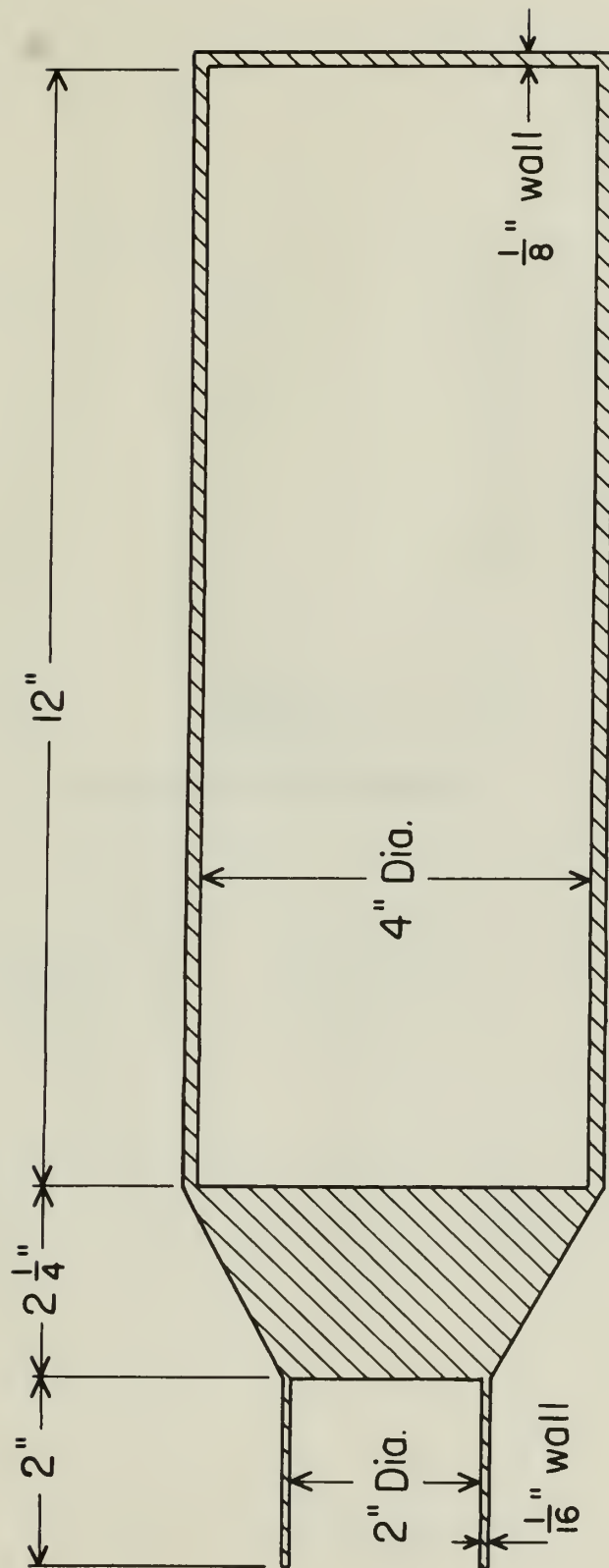


Figure 4



Figure 5  
Electronics Block Diagram

Figure 2  
 Illustration of the diagram



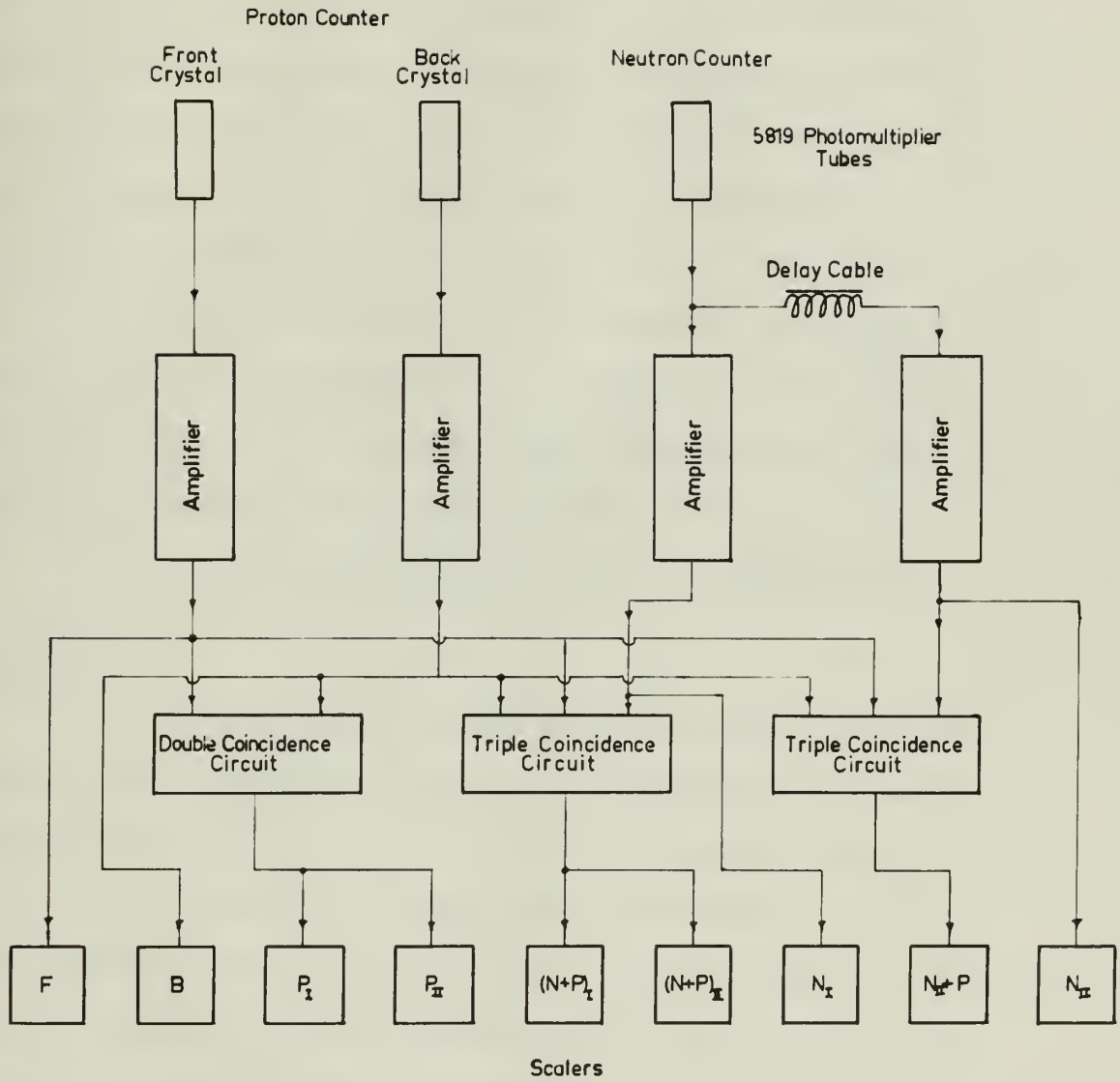


Figure 5



employed on the amplifiers to select the pulse height to be observed. The channels for the front and back crystals of the proton telescope are connected through a (two-fold) coincidence circuit to give the proton count. The neutron signals were sent to the regular neutron channel (Neutrons<sub>I</sub>) and also through a 56 meter (0.3 microsecond) RG-63/U cable to another amplifier channel (Neutrons<sub>II</sub>) for measuring the accidental counting rate. Each of these neutron channels was connected to a separate triple coincidence circuit with the front and back crystals of the proton counter. This arrangement gave the total neutron-proton coincidence rate and simultaneously the accidental neutron-proton coincidence rate. As a check two scalars were employed on the proton and the neutron-proton coincidence channels. The resolving time,  $2\tau$ , of the coincidence circuits was about 0.17 microseconds.

#### D. Targets

The targets employed in this work were water, heavy water, lithium, carbon, aluminum and copper. A description of the targets is found in Table II. It was desired to have targets of exactly the same energy loss for 130 Mev protons (i.e.  $\Delta E = 20$  Mev). However, time limitations compelled the use of the targets at hand with the result that this condition was not always realized. The energy losses for targets perpendicular to the proton counter are listed in column 5 of table II.

A special lithium metal target was cast in a dry box under a helium atmosphere. Due to uneven contraction on cooling it had to

employed on the amplifier to adjust the pulse height to be observed. The channels for the front and back crystals of the proton detector are connected through a (two-fold) coincidence circuit to give the proton count. The neutron signals were sent to the regular neutron channel (Neutron<sub>I</sub>) and also through a 50 meter (0.3 microseconds) RC- $\delta$  V cable to another amplifier channel (Neutron<sub>II</sub>) for measuring the accidental counting rate. Each of these neutron channels was connected to a separate triple coincidence circuit with the front and back crystals of the proton counter. This arrangement gave the total neutron-proton coincidence rate and simultaneously the accidental neutron-proton coincidence rate. As a check two meters were employed on the proton and the neutron-proton coincidence channels. The resolving time,  $\tau$ , of the coincidence circuit was about 0.17 microseconds.

## II. Targets

The targets employed in this work were water, heavy water, lithium, carbon, aluminum and copper. A description of the targets is found in Table II. It was desired to have targets of exactly the same energy loss for 150 Mev protons (i.e.,  $\Delta E = 50$  Mev). However, time limitations compelled the use of the targets at hand with the result that this condition was not always realized. The energy losses for targets perpendicular to the proton counter are listed in column 2 of Table II.

A special lithium metal target was cast in a dry box under a helium atmosphere. One to seven contractions on cooling it led to



TABLE II

## Target Data

Substance	Z	A	Target Thickness m/cm <sup>2</sup>	Energy Loss( $\Delta E$ ) for 130 Mev pro- tons(Mev)	Target Angle		
					$\theta_N^*$	$\theta_T$ for $\theta_N$	$\theta_T$ for $\theta_N$
Lithium	3	6.94	1.90	10.5	100	134	63
Carbon	6	12.01	3.10	18.0	96	140	50
Light Water			2.18	17		140	Not run above 100
Heavy Water			2.35	19		140	
Aluminum	13	26.98	3.35	17.2	100	140	50
Copper	29	63.54	4.38	19.2	96	140	50

\* $\theta_N$  is the neutron counter angle at which the target angle is shifted.



be machined to a thickness thinner than that anticipated in order to obtain a uniform surface. It was wrapped in thin aluminum foil, and the seams were dipped in paraffin.

The heavy water and light water targets were in thin walled plastic cells. Unfortunately the tension was different in the walls of the two cells. This led to the  $H_2O$  cell being 2 percent thicker than the  $D_2O$  cell. The other samples were bare metal plates. All targets were larger than the beam.

In general targets were set at about 140 degrees to the beam. In order to keep the neutron scattering negligible in the target, the target angle was shifted to about 40 degrees when the neutron counter was at angles larger than about 100 degrees.

As pointed out in Christie's<sup>31</sup> analysis of the deuterium data, the finite size of the target adds to the angular resolution associated with the geometry. It was desired to keep the angular resolution the same for the various elements. A graphical analysis was made of the projection (on a perpendicular to the axis of the proton telescope) of the beam's intersection with the target. This was a function of the thickness of the target. The criterion chosen was that the proton telescope should observe a three inch projection of the portion of the target in the beam.

The angles used for the various targets are listed in the last columns of Table II. The sixth column lists the neutron counter angle at which the target angle was shifted. These angles were set



be measured to a thickness of about 100 microns in order to obtain a uniform surface. It was covered in thin aluminum foil, and the beam was directed in parallel.

The heavy water and light water targets were in thin walled plastic cells. Unfortunately the reaction was different in the walls of the two cells. This led to the  $H_2O$  cell being 2 percent thicker than the  $D_2O$  cell. The other samples were made of glass. All targets were larger than the beam.

In general targets were set at about 100 degrees to the beam. In order to keep the neutron scattering negligible in the target, the target angle was shifted to about 40 degrees when the neutron source was at angles larger than about 100 degrees. As pointed out in Chapter II, the analysis of the reaction data.

the choice of the target angle to the angular resolution associated with the geometry. It was desired to keep the angular resolution the same for the various elements. A graphical analysis was made of the projection (on a perpendicular to the axis of the proton telescope) of the beam's intersection with the target. This was a function of the elements of the target. The analysis showed that the proton telescope should observe a three inch projection of the position of the target in the beam.

The angles used for the various targets are listed in the last column of Table II. The third column lists the neutron source angle at which the target angle was shifted. These angles were 200





although about one degree out of position that was contained in the beam.  
The position was corrected by means of a very photostatic of the beam.

The position of the beam

The beam was not perfectly horizontal, as will be seen

from the photograph. The position of the beam was

not perfectly horizontal, as will be seen from the photograph.

The position of the beam was not perfectly horizontal, as will be seen

from the photograph. The position of the beam was

not perfectly horizontal, as will be seen from the photograph.

The position of the beam was not perfectly horizontal, as will be seen

from the photograph. The position of the beam was

not perfectly horizontal, as will be seen from the photograph.

The position of the beam was not perfectly horizontal, as will be seen

from the photograph. The position of the beam was

not perfectly horizontal, as will be seen from the photograph.

The position of the beam was not perfectly horizontal, as will be seen

from the photograph. The position of the beam was

not perfectly horizontal, as will be seen from the photograph.

The position of the beam was not perfectly horizontal, as will be seen

from the photograph. The position of the beam was

not perfectly horizontal, as will be seen from the photograph.

The position of the beam was not perfectly horizontal, as will be seen

from the photograph. The position of the beam was

not perfectly horizontal, as will be seen from the photograph.

### III Experimental Procedure

#### A. Standards

Radioactive sources were employed as standards in order to minimize drift of the high voltage supplies and other electronic components. On the proton telescope the brass absorber was removed and the 500 microcurie radium source was suspended at the center of the target side of the front collimator opening. The counting rates of both the front and back crystals were observed. The neutron counter was standardized by inserting a 2 microcurie cobalt-60 source inside the cylindrical lead shield to the mid-point of the counter, and reading the counting rate on the normal neutron channel ( $\text{Neutrons}_I$ ). Adjustments were made by varying the high voltage on the photomultiplier tubes. All discriminator bias settings on the amplifiers were fixed with a potentiometer. Voltage readings were made with an electrostatic voltmeter.

#### B. Treatment of Accidentals

As previously mentioned an evaluation of the number of accidental neutron-proton coincidences was made by employing a delayed neutron channel in coincidence with the front and back channels of the proton counter. The delayed neutron channel ( $\text{Neutrons}_{II}$ ) was generally run at a lower bias and hence higher counting rate than the normal neutron channel ( $\text{Neutrons}_I$ ) to obtain better statistics. The accidental neutron-proton counts were normalized to the normal neutron-



### III. Experimental Procedure

#### A. Apparatus

Radioactive sources were employed as standards in order to obtain a calibration of the high voltage supplies and other electronics components. In the present experiment the probe detector was removed and the 500 microcurie radium source was suspended at the center of the target side of the front collision chamber. The counting rates of both the front and back crystals were observed. The neutron monitor was substituted by inserting a 2 microcurie cobalt-60 source inside the cylindrical lead shield to the midpoint of the monitor, and reading the counting rate on the normal neutron channel (Neutron<sub>I</sub>). Adjustments were made by varying the high voltage on the photomultiplier tubes. All discriminator bias settings on the amplifiers were fixed with a potentiometer. Voltage readings were made with an electrostatic voltmeter.

#### B. Treatment of Data

As previously mentioned in connection with the number of scattered neutron-proton coincidences was made by analyzing a delayed neutron channel in coincidence with the front and back channels of the probe counter. The delayed neutron channel (Neutron<sub>II</sub>) was generally run at a lower bias and hence higher counting rate than the normal neutron channel (Neutron<sub>I</sub>) to obtain better statistics. The scattered neutron-proton counts were corrected to the normal neutron-



proton counts by the following proportion:

$$\frac{(N_{\pi+p})_{\text{normalized}}}{N_{\pi+p}} = \frac{N_{\pi}}{N_{\pi}}$$

The normalized accidental counts were then subtracted from the total neutron-proton counts to give the true number of neutron-proton coincidences for the run.

### C. Kinematics

Employing relativistic momentum and energy conservation the proton counter energy and angle were set so as to make the proton angle 90 degrees in the center of mass coordinates of the deuteron<sup>14</sup>. For 130 Mev protons this angle in the laboratory was 76 degrees. This meant the neutron angle in center of mass coordinates was 90 degrees with the consequence that it would also be 76 degrees in the laboratory. However, due to the finite size of the target and orientation relative to the two counters the peak of the neutron angular distribution should occur at a slightly larger angle as shown by Christie<sup>31</sup>. The observed peak of the neutron angular distribution occurred at 78 degrees in the laboratory coordinates.

### D. Description of Runs

Runs were normally made first at a (protractor) setting of 73 degrees for the neutron counter. This was followed by a run on either side for the "wings" of the neutron angular distribution, and then by runs at ten degree increments to establish the shape of the distribution. One or more subsequent runs were made at 78 degrees as a check on

proton counts by the following proportion:

$$\frac{N_{\text{p}}}{N_{\text{p}+n}} = \frac{N_{\text{p}+n}(\text{corrected})}{N_{\text{p}+n}}$$

The normalized scattered counts were then subtracted from the total

neutron-proton counts to give the true number of neutron-proton

scattering for the run.

### C. Limitation

Applying relativistic momentum and energy conservation the

proton counter energy and angle were set so as to make the proton

angle 90 degrees in the center of mass coordinates of the detector.<sup>14</sup>

For 130 kev protons this angle in the laboratory was 70 degrees. This

meant the neutron angle in center of mass coordinates was 90 degrees

when the consequence that it would also be 90 degrees in the laboratory.

However, due to the finite size of the target and orientation relative

to the two counters the peak of the neutron angular distribution would

occur at a slightly larger angle as shown by Chart 11.<sup>15</sup> The observed

peak of the neutron angular distribution occurred at 78 degrees in the

laboratory coordinate.

### D. Position of Run

Runs were normally made first at a (proton) setting of 78

degrees for the neutron counter. This was followed by a run on either

side for the "shape" of the neutron angular distribution, and then by

runs at two degree increments to establish the shape of the distribution.

One or more subsequent runs were made at 70 degrees to a check on





"role" Larry told to telephone at not when was and "unlike"

for plotting data.



#### IV. Analysis of Data

##### A. Reduction of Raw Data

A typical set of readings is shown in Table III to illustrate the information recorded in each run. Each count reading was divided by the number of "mice"\* as a check on reproducibility. Summary tables of the data for each element were made up. The more important parts of these are reproduced in Tables IVa through IVf. These tables show the actual total counts observed and are not normalized for the number of "mice" in each run. The last column of each table gives the corrected coincidence counts divided by the proton count. Ideally the proton count should have been a constant. By dividing by the proton rate, we are correcting for the necessary changes in target position, drifts in the proton counter, drifts in the machine energy and intensity, errors in the placement of the target, errors in the monitoring system and variations in the number of "mice" per run. The values of the  $\frac{N+P}{P}$  ratios were generally almost always reproducible within statistics when the points were rerun.

##### B. Deuterium

The neutron-proton coincidences in heavy water are assumed to be due to both the deuterium and the oxygen while those from light water are due only to the oxygen. A subtraction performed according to the following formula gave the desired values for deuterium:

$$\frac{(N+P)_{D_2O} - 0.98 (N+P)_{H_2O}}{P_{ave} D_2O - 0.98 P_{ave} H_2O}$$

\*See Section IIID.

# IV. Analysis of Data

## A. Evaluation of Raw Data

A typical set of readings is shown in Table III to illustrate the information recorded in each run. Each count reading was divided by the number of "hits" as a check on reproducibility. Summary tables of the data for each element were made up. The more important parts of these are reproduced in Tables IVa through IVc. These tables show the actual total counts obtained and are not corrected for the number of losses in each run. The last column of each table gives the corrected coincidence counts divided by the proton count. Ideally the proton count would have been a constant. If divided by the proton rate, we are correcting for the necessary changes in target position, drifts in the proton current, drifts in the neutron counter and intensity, errors in the placement of the target, errors in the scattering angle and variations in the number of "hits" per run. The value of the  $\frac{1}{2}$  ratios were generally about unity reproducibly within statistical limits when the points were taken.

## B. Discussion

The neutron-proton coincidences in heavy water are assumed to be due to both the deuteron and the oxygen while those from light water are due only to the oxygen. A comparison between the two the following formula gave the desired values for deuterium

$$\frac{D_2O}{H_2O} = \frac{D_2O(1.00) - 0.02(H_2O)}{D_2O(1.00) - 0.02(H_2O)}$$



TABLE III  
Samples of Data Recorded During Runs

Mice*	Target	Counter Angles		Target Angle (Q <sub>T</sub> )	Front Channel Clicks <sup>#</sup> (F)	Back Channel Count <sup>#</sup> (B)	Proton Counts <sup>#</sup>		Neutron Clicks <sup>#</sup>		Neutron-Proton Coincidence Counts <sup>#</sup>		
		Proton (Q <sub>P</sub> )	Neutron (Q <sub>N</sub> )				Scaler I (P <sub>I</sub> )	Scaler II (P <sub>II</sub> )	Normal (N <sub>I</sub> )	Delayed (N <sub>II</sub> )	Total		Delayed (N <sub>II</sub> +P)
1500	C	76	88	140	0686 0026 660	6333 <sup>12</sup> 6159 11148	839 <sup>9</sup> 717 7753	160 <sup>7</sup> 040 7687	3849 3425 424	3656 3166 490	72 <sup>22</sup> 72 22	00 <sup>22</sup> 00 22	61 <sup>8</sup> 61 8
Counts/mouse					0.440	7.44	5.17	5.13	0.283	0.327	0.0147	0.0147	0.0053
3000	C	76	88	140	1336 0026 1310	6507 <sup>53</sup> 6159 22325	959 <sup>31</sup> 717 15519	280 <sup>25</sup> 040 15385	4257 3425 832	5782 3166 2616	72 <sup>48</sup> 72 48	00 <sup>48</sup> 00 48	61 <sup>9</sup> 61 9
Counts/mouse					0.437	7.44	5.18	5.13	0.277	0.872	0.016	0.016	0.003
1500	C	76	108	50	1887 1336 551	6653 <sup>45</sup> 6508 9325	061 <sup>7</sup> 959 6535	381 <sup>39</sup> 280 6503	4607 4337 270	7481 5788 1693	73 <sup>7</sup> 73 7	00 <sup>7</sup> 00 7	61 <sup>4</sup> 61 4
Counts/mouse					0.367	6.22	4.36	4.33	0.180	1.13	0.0047	0.0047	0.0027
3000	C	76	108	50	2421 1336 1085	6797 <sup>3</sup> 6508 18499	160 <sup>32</sup> 959 12926	480 <sup>59</sup> 280 12859	4866 4337 529	9105 5188 3317	73 <sup>15</sup> 73 15	00 <sup>15</sup> 00 15	61 <sup>6</sup> 61 6
Counts/mouse					0.362	6.17	4.31	4.29	0.176	1.11	0.005	0.005	0.002

\* See Section III D

# Scale of 64 scalars were used. When counting rates sufficiently high only the number of clicks was recorded. 1 click = 64 counts.

Runs were generally stopped in the middle and readings taken as a check on reproducibility

TABLE 1. - *Continued*

Station	Depth (m)	Temperature (°C)	Salinity (‰)	Density (σ <sub>t</sub> )	Specific Gravity	Notes
1000	1000	10.5	35.0	1.024	1.024	
	1000	10.5	35.0	1.024	1.024	
2000	2000	10.5	35.0	1.024	1.024	
	2000	10.5	35.0	1.024	1.024	
3000	3000	10.5	35.0	1.024	1.024	
	3000	10.5	35.0	1.024	1.024	
4000	4000	10.5	35.0	1.024	1.024	
	4000	10.5	35.0	1.024	1.024	
5000	5000	10.5	35.0	1.024	1.024	
	5000	10.5	35.0	1.024	1.024	

Notes: - The density of the water was determined from the temperature and salinity readings. The specific gravity was determined from the density. The temperature was determined from the thermistor readings. The salinity was determined from the conductivity readings. The density was determined from the temperature and salinity readings. The specific gravity was determined from the density. The temperature was determined from the thermistor readings. The salinity was determined from the conductivity readings.



TABLE IVa

## Summary of Heavy Water Data

Neutron Counter Angle ( $\theta_N$ )	Proton Counts ( $P_I$ )	Neutron - Proton Coincidences		
		Total ( $N+P$ )	Corrected <sup>②</sup>	Normalized <sup>#</sup> Corrected
63	12224	37	29.6	$24 \pm 5$
68	12180	68	62.5	$51 \pm 7$
73	12610	127	121.2	$96 \pm 9$
78	12235	132	126.7	$103 \pm 10$
78	12669	146	140.2	$111 \pm 10$
*78	24904	278	266.8	$107 \pm 7$
83	12600	79.5	76.1	$60 \pm 7$
83	13546	93	87.7	$65 \pm 7$
*83	26146	172.5	163.8	$63 \pm 5$
88	12245	47	43.5	$36 \pm 6$
88	12821	43	37.7	$29 \pm 5$
*88	25066	90	81.1	$32 \pm 4$
Ave	12570			

② Corrected Neutron-Proton Coincidences =  $(N+P) - (N_{II}+P) \frac{N_I}{N_{II}}$

# Normalized, corrected neutron-proton coincidences =  $\frac{1}{P_I} \times$  Corrected Coincidences

\* Combination of runs above at same angle

Taken with proton counter at  $76 \pm 5$  degrees and with proton energy of  $130 \pm 12$  Mev.

See Table II for data on Target

TABLE IV

Summary of Heavy Water Data

Neutron Counter Reading ( $\times 10^3$ )	Neutron Count ( $\times 10^3$ )	Neutron - Proton Coincidence		
		Corrected	Observed	Uncorrected
25	1250	37	20.6	26 $\pm$ 2
30	1350	46	22.2	27 $\pm$ 2
35	1450	57	22.2	28 $\pm$ 2
40	1550	68	22.7	29 $\pm$ 2
45	1650	79	22.2	30 $\pm$ 2
50	1750	89	22.6	30 $\pm$ 2
55	1850	99	22.1	30 $\pm$ 2
60	1950	109	22.7	31 $\pm$ 2
65	2050	119	22.2	31 $\pm$ 2
70	2150	129	22.2	31 $\pm$ 2
75	2250	139	22.7	32 $\pm$ 2
80	2350	149	22.2	32 $\pm$ 2
85	2450	159	22.7	32 $\pm$ 2
90	2550	169	22.2	32 $\pm$ 2
95	2650	179	22.7	32 $\pm$ 2
100	2750	189	22.2	32 $\pm$ 2

Corrected Neutron-Proton Coincidence =  $(N_p^2) - (N_p^2) \times \frac{1}{11}$

Uncorrected Neutron-Proton Coincidence =  $\frac{1}{11} \times$  Corrected

\* Coincidence of same phase of wave signal

Values with proton counter at 70  $\pm$  5 degrees and with proton energy of 1.0  $\pm$  0.1 MeV.

See Table II for data on target

TABLE IVb

## Summary of Lithium Data

Neutron Counter Angle (°)	Proton Counts (P <sub>I</sub> )	Neutron - Proton Coincidences		
		Total (N+P)	Corrected <sup>⊗</sup>	Normalized <sup>#</sup> Corrected
38	4505	3	1.6	4± 5
48	6829	6	4.7	7± 4
58	6798	26	26	38± 8
68	4516	45	40.9	91± 16
78	4476	49	47.6	106± 16
78	3344	27	25.6	77± 16
78	3960	32	30.7	78± 15
*78	11780	108	103.9	88± 9
88	6407	34	28.6	45± 10
98	8187	24	24	29± 6
108	7471	8	8	11± 4
118	3958	2	0.5	1± 5

$$\text{⊗ Corrected Neutron-Proton Coincidences} = (N+P) - (N_{II} + P) \frac{N_I}{N_{II}}$$

$$\text{# Normalized corrected neutron-proton coincidences} = \frac{1}{P_I} \times \text{Corrected Coincidences}$$

\* Combination of runs above at same angle

Taken with proton counter at  $76 \pm 5$  degrees and with proton energy of  $130 \pm 12$  Mev.

See Table II for data on Target



TABLE IV

Summary of Results

Run	Protein Conc. (%)	Protein Conc. (%)	Protein-Protein Conc. (%)	
			Protein Conc. (%)	Protein Conc. (%)
1	0.2	0.2	0.2	0.2
2	0.5	0.5	0.5	0.5
3	1.0	1.0	1.0	1.0
4	2.0	2.0	2.0	2.0
5	4.0	4.0	4.0	4.0
6	8.0	8.0	8.0	8.0
7	16.0	16.0	16.0	16.0
8	32.0	32.0	32.0	32.0
9	64.0	64.0	64.0	64.0
10	128.0	128.0	128.0	128.0
11	256.0	256.0	256.0	256.0
12	512.0	512.0	512.0	512.0
13	1024.0	1024.0	1024.0	1024.0
14	2048.0	2048.0	2048.0	2048.0
15	4096.0	4096.0	4096.0	4096.0
16	8192.0	8192.0	8192.0	8192.0
17	16384.0	16384.0	16384.0	16384.0
18	32768.0	32768.0	32768.0	32768.0
19	65536.0	65536.0	65536.0	65536.0
20	131072.0	131072.0	131072.0	131072.0
21	262144.0	262144.0	262144.0	262144.0
22	524288.0	524288.0	524288.0	524288.0
23	1048576.0	1048576.0	1048576.0	1048576.0
24	2097152.0	2097152.0	2097152.0	2097152.0
25	4194304.0	4194304.0	4194304.0	4194304.0
26	8388608.0	8388608.0	8388608.0	8388608.0
27	16777216.0	16777216.0	16777216.0	16777216.0
28	33554432.0	33554432.0	33554432.0	33554432.0
29	67108864.0	67108864.0	67108864.0	67108864.0
30	134217728.0	134217728.0	134217728.0	134217728.0
31	268435456.0	268435456.0	268435456.0	268435456.0
32	536870912.0	536870912.0	536870912.0	536870912.0
33	1073741824.0	1073741824.0	1073741824.0	1073741824.0
34	2147483648.0	2147483648.0	2147483648.0	2147483648.0
35	4294967296.0	4294967296.0	4294967296.0	4294967296.0
36	8589934592.0	8589934592.0	8589934592.0	8589934592.0
37	17179869184.0	17179869184.0	17179869184.0	17179869184.0
38	34359738368.0	34359738368.0	34359738368.0	34359738368.0
39	68719476736.0	68719476736.0	68719476736.0	68719476736.0
40	137438953472.0	137438953472.0	137438953472.0	137438953472.0
41	274877906944.0	274877906944.0	274877906944.0	274877906944.0
42	549755813888.0	549755813888.0	549755813888.0	549755813888.0
43	1099511627776.0	1099511627776.0	1099511627776.0	1099511627776.0
44	2199023255552.0	2199023255552.0	2199023255552.0	2199023255552.0
45	4398046511104.0	4398046511104.0	4398046511104.0	4398046511104.0
46	8796093022208.0	8796093022208.0	8796093022208.0	8796093022208.0
47	17592186044416.0	17592186044416.0	17592186044416.0	17592186044416.0
48	35184372088832.0	35184372088832.0	35184372088832.0	35184372088832.0
49	70368744177664.0	70368744177664.0	70368744177664.0	70368744177664.0
50	140737488355328.0	140737488355328.0	140737488355328.0	140737488355328.0

$$\frac{1}{II} \frac{d}{dt} \ln \left( \frac{P}{P_0} \right) = (k_p - k_{-p}) \frac{P}{P_0}$$

$$\ln \left( \frac{P}{P_0} \right) = (k_p - k_{-p}) \frac{P}{P_0} \times \frac{1}{II}$$

\* Combination of two steps of same order  
 † Data with protein content at 10% & 20% and with protein  
 content of 1.0% & 1.5%  
 ‡ See Table II for data on larger



TABLE IVc

## Summary of Carbon Data

Neutron Counter Angle ( $\theta_N$ )	Proton Counts ( $P_I$ )	Neutron - Proton Coincidences		
		Total ( $N+P$ )	Corrected <sup>a</sup>	Normalized <sup>#</sup> Corrected
38	13248	14	8.4	$6.3 \pm 2.9$
48	8020	9	8.0	$10 \pm 4$
58	13785	30	26.1	$19 \pm 4$
68	13684	43	38.9	$28 \pm 5$
78	13298	53	46.3	$35 \pm 6$
78	15385	53	51.6	$34 \pm 5$
*78	28683	106	101.8	$36 \pm 4$
88	15519	48	45.1	$29 \pm 5$
98	12480	24	22.6	$18 \pm 4$
108	12926	15	14.0	$11 \pm 3$
118	20300	15	11.8	$5.8 \pm 1.9$
128	12129	2	2	$1.6 \pm 1.6$

<sup>a</sup> Corrected Neutron-Proton Coincidences =  $(N+P) - (N_{II}+P) \frac{N_I}{N_{II}}$

<sup>#</sup> Normalized corrected neutron-proton coincidences =  $\frac{1}{P_I} \times \text{Corrected Coincidences}$

\*Combination of runs above at same angle

Taken with proton counter at  $76 \pm 5$  degrees and with proton energy of  $130 \pm 12$  Mev.

See Table II for data on Target



TABLE IVd

## Summary of Light Water (Oxygen) Data

Neutron Counter Angle ( $\theta_N$ )	Proton Counts ( $P_I$ )	Neutron - Proton Coincidences		
		Total (N+P)	Corrected <sup>a</sup>	Normalized Corrected <sup>#</sup>
68	10694	32	26.2	$25 \pm 5$
78	10527	46	38.1	$36 \pm 7$
88	10646	25	22.4	$21 \pm 5$
ave	10622			

<sup>a</sup> Corrected Neutron-Proton Coincidences =  $(N P) - (N_{II} P) \frac{N_I}{N_{II}}$

<sup>#</sup> Normalized corrected neutron-proton coincidences =  $\frac{1}{P_I} \times$  Corrected Coincidences

Taken with proton counter at  $76 \pm 5$  degrees and with proton energy of  $130 \pm 12$  Mev.

See Table II for data on Target



TABLE IV

Summary of Light Water (LWR) Data

Reaction Counter Rate (%)	Proton Count (%)	Left (%)	Right - Proton Coincidence
60	100%	30	2 ± 2
70	100%	40	6 ± 2
80	100%	50	11 ± 2
ave	100%		

$$\text{Corrected Reaction-Proton Coincidence} = (N_R) - (N_L) \pm \frac{N_L}{N_{II}}$$

$$\text{Normalized corrected reaction-proton coincidence} = \frac{1}{N_{II}} \times \text{Coincidence}$$

Values with proton number of 70 ± 2 denote and with proton number of 100 ± 10 den.

See Table II for data on LWR



TABLE IVe  
Summary of Aluminum Data

Neutron Counter Angle ( $\theta_N$ )	Proton Counts ( $P_I$ )	Neutron - Proton Coincidences		
		Total ( $N+P$ )	Corrected <sup>Ⓢ</sup>	Normalized <sup>#</sup> Corrected
38	14663	25	15.1	$10 \pm 4$
58	15104	19	13.6	$9 \pm 3$
68	14577	35	30.4	$21 \pm 4$
78	14464	37	32.9	$23 \pm 4$
78	14205	40	35.9	$25 \pm 5$
*78	28669	77	68.8	$24 \pm 3$
88	13963	27	23.4	$17 \pm 4$
88	14135	36	32.4	$23 \pm 5$
*88	28098	63	55.8	$20 \pm 3$
98	12620	28	25.1	$20 \pm 4$
98	12646	18	15.1	$12 \pm 4$
*98	25266	46	40.2	$15.9 \pm 2.8$
108	12717	14	11.3	$9 \pm 3$
118	12975	12	9.5	$7.3 \pm 2.9$
128	12556	9	6.7	$5.3 \pm 2.7$

Ⓢ Corrected Neutron-Proton Coincidences =  $(N+P) - 0.005 N_I$

# Normalized corrected neutron-proton coincidences =  $\frac{1}{P_I} \times \text{Corrected Coincidences}$

\*Combination of runs above at same angle

Taken with proton counter at  $76 \pm 5$  degrees and with proton energy of  $130 \pm 12$  Mev.

See Table II for data on Target

TABLE IV  
Summary of Atomic Data

Neutron Number (N)	Atomic Number (Z)	Neutron - Proton Coincidence	
		Counted	Normalized
28	14.02	32	12.1
29	12.10	18	13.2
30	12.77	37	30.4
31	14.04	27	12.8
32	14.00	40	12.9
33	20.60	73	18.8
34	13.93	57	41.4
35	14.13	36	30.4
36	20.94	63	27.8
37	12.30	28	27.7
38	13.68	18	12.1
39	22.84	66	40.2
40	12.75	14	11.3
41	12.97	15	0.2
42	12.28	9	0.2

\* Corrected neutron-proton coincidence = (N/P) — 0.002 N

\* Normalized corrected neutron-proton coincidence =  $\frac{1}{N} \times$  (Corrected coincidence)

\* Coincidence of two above 45 degrees

\* Taken with proton counter at  $70 \pm 2$  degrees and with proton energy of  $130 \pm 15$  MeV.

\* See Table II for data on target



TABLE IVf

## Summary of Copper Data

Neutron Counter Angle ( $\theta_N$ )	Proton Counts ( $P_I$ )	Neutron - Proton Coincidences		
		Total (N P)	Corrected <sup>a</sup>	Normalized <sup>#</sup> Corrected
38	10556	15	(-) 9.7	(-) 9 $\pm$ 5
48	13929	16	10.4	7.5 $\pm$ 2.9
58	17493	29	22.9	13 $\pm$ 3
68	16197	35	32.3	20 $\pm$ 4
73	16451	27	23.5	14 $\pm$ 3
78	10800	16	14.9	14 $\pm$ 4
78	17166	38	34.0	20 $\pm$ 4
*78	27966	54	50.1	17.9 $\pm$ 2.7
88	16714	34	30.3	18 $\pm$ 3
98	16159	20	17.0	10.5 $\pm$ 2.9
108	16273	8	6.3	3.9 $\pm$ 1.8
118	16064	2	1.1	0.7 $\pm$ 0.9
128	15543	8	4.8	3.1 $\pm$ 1.9

<sup>a</sup> Corrected Neutron-Proton Coincidences =  $(N P) - (N_{II} P) \frac{N_I}{N_{II}}$

<sup>#</sup> Normalized corrected neutron-proton coincidences =  $\frac{1}{P_I} \times \text{Corrected Coincidences}$

\* Combination of runs above at same angle

Taken with proton counter at  $76 \pm 5$  degrees and with proton energy of  $130 \pm 12$  Mev.

See Table II for data on Target

University of Oxford, Dec.

[illegible]
$$\frac{1}{r_1} (q_{II}^n) - (q_{II}^n) = \text{corrected } \text{H}_2\text{O} \text{ corrected } \text{H}_2\text{O}$$
$$\text{Correlation coefficient} = \frac{1}{n} \sum_{i=1}^n \frac{(x_i - \bar{x})(y_i - \bar{y})}{\sqrt{(x_i - \bar{x})^2 (y_i - \bar{y})^2}}$$

signs and to avoid any "collateral"

1945

See Table II for data on Program



The factor 0.98 compensated for the different target thicknesses explained in Section II D. The reduction of data according to the above formula is illustrated in Table V. The denominator is an approximately 20 percent difference between the two proton rates. The denominator was obtained by averaging the proton rates at all angles. Despite this the error in the denominator for deuterium still was commensurate with the errors in the numerator at the various angles.

As the  $H_2O$  curve was fairly flat in the region of interest for deuterium previous experience had shown it was not necessary to run  $H_2O$  at every angle for the information desired in this experiment. Consequently, as all that was desired of the deuterium curve was to check the resolution of the geometry employed in these measurements the  $H_2O$  target was run only at 68, 78 and 88 degrees. The remaining data was filled in from two previously determined oxygen curves with almost identical geometries.

### C. Resolution of Equipment

If the target had been infinitesimal in size the finite size of the proton counter and the neutron counter would have given a triangular resolution curve of about 10 degrees width at half height. The peak height from deuterium obtained in this case would have been the efficiency of the neutron counter  $\left( \frac{\Delta N + P}{\Delta P} \right)$ . Christie<sup>31</sup> has shown that the finite size of the target spreads out the resolution of the detecting system to about 14 degrees. The peak height is also decreased by the target size.

The factor 0.98 corresponds to the different target thicknesses explained in section II.6. The radiation of data recorded to the above formula is illustrated in Table V. The denominator is an approximately 20 percent difference between the two proton rates. The denominator was obtained by averaging the proton rates in all angles. Despite this the error in the denominator for detection with was comparable with the error in the numerator at the various angles. As the  $H_2O$  curve was fairly flat in the region of interest for detection previous experiments had shown it was not necessary to run  $H_2O$  at every angle for the information desired in this experiment. Consequently, as all that was desired of the detecting system was to check the resolution of the geometry employed in these experiments the  $H_2O$  target was run only at 40, 48 and 50 degrees. The resulting data was fitted to two low previously determined oxygen curves with almost identical resolution.

### C. Resolution of Geometry

If the target had been infinitesimal in size the limits of the proton counter and the neutron counter would have given a rectangular resolution curve of width 10 degrees with a half height. The peak height from detection obtained in this case would have been the ellipticity of the neutron counter  $\left(\frac{4\pi}{3} \frac{A}{Z} \right)$ . Christie<sup>12</sup> has shown that the finite size of the target provides not the resolution of the detecting system to about 10 degrees. The peak height is also decreased by the target size.



TABLE V  
Reduction of Data for Deuterium From  $D_2O$  and  $H_2O$

Neutron Counter Angle $\Theta_N$	Neutron-Proton Coincidences				Average Proton Counts				Virtual Deuterium Coincidences $\times 10^3$
	$D_2O^\oplus$	$H_2O$	$0.98H_2O$	Difference $D_2O-0.98 H_2O$	$D_2O^\dagger$	$H_2O^\&$	$0.98 H_2O$	Differences $D_2O-0.98H_2O$	
63	29.6		25.1 <sup>#</sup>	8.1	12570	10622	10410	2160	3.8 $\pm$ 4.0
68	62.5	26.2	25.7 <sup>*</sup>	36.8	"	"	"	"	17.0 $\pm$ 4.7
73	121.2		35.8 <sup>#</sup>	85.4	"	"	"	"	40 $\pm$ 6
78	133.4	38.1	37.3 <sup>*</sup>	96.1	"	"	"	"	45 $\pm$ 5
83	81.9		35.8 <sup>#</sup>	46.1	"	"	"	"	21.4 $\pm$ 4.1
88	40.6	22.4	22.0 <sup>*</sup>	18.6	"	"	"	"	8.6 $\pm$ 3.2

⊙ From Column 4, Table IVa

# From previous oxygen data

\* From Column 4, Table IVd

† See Table IVa

& See Table IVc

All data normalized to 3000 Mice

$$\text{Column 10} = \frac{(N_P)_{D_2O} - 0.98 (N_P)_{H_2O}}{\text{Pave } D_2O - 0.98 \text{ Pave } H_2O} \times 10^3$$

# 7 SHEET

Q<sub>2</sub>W has Q<sub>2</sub>Q and is not to be used

Cust. Ref. No. (1-1000) Q <sub>2</sub> W	Elementary nodes				Secondary nodes				Remarks
	Q <sub>2</sub> W	Q <sub>2</sub> W	Q <sub>2</sub> W	Q <sub>2</sub> W	Q <sub>2</sub> W	Q <sub>2</sub> W	Q <sub>2</sub> W	Q <sub>2</sub> W	
0.1 ± 0.1	Q <sub>2</sub> W	Q <sub>2</sub> W	Q <sub>2</sub> W	Q <sub>2</sub> W	Q <sub>2</sub> W	Q <sub>2</sub> W	Q <sub>2</sub> W	Q <sub>2</sub> W	Q <sub>2</sub> W
1.1 ± 0.1	Q <sub>2</sub> W	Q <sub>2</sub> W	Q <sub>2</sub> W	Q <sub>2</sub> W	Q <sub>2</sub> W	Q <sub>2</sub> W	Q <sub>2</sub> W	Q <sub>2</sub> W	Q <sub>2</sub> W
2.1 ± 0.1	Q <sub>2</sub> W	Q <sub>2</sub> W	Q <sub>2</sub> W	Q <sub>2</sub> W	Q <sub>2</sub> W	Q <sub>2</sub> W	Q <sub>2</sub> W	Q <sub>2</sub> W	Q <sub>2</sub> W
3.1 ± 0.1	Q <sub>2</sub> W	Q <sub>2</sub> W	Q <sub>2</sub> W	Q <sub>2</sub> W	Q <sub>2</sub> W	Q <sub>2</sub> W	Q <sub>2</sub> W	Q <sub>2</sub> W	Q <sub>2</sub> W
4.1 ± 0.1	Q <sub>2</sub> W	Q <sub>2</sub> W	Q <sub>2</sub> W	Q <sub>2</sub> W	Q <sub>2</sub> W	Q <sub>2</sub> W	Q <sub>2</sub> W	Q <sub>2</sub> W	Q <sub>2</sub> W
5.1 ± 0.1	Q <sub>2</sub> W	Q <sub>2</sub> W	Q <sub>2</sub> W	Q <sub>2</sub> W	Q <sub>2</sub> W	Q <sub>2</sub> W	Q <sub>2</sub> W	Q <sub>2</sub> W	Q <sub>2</sub> W

Q<sub>2</sub>W has Q<sub>2</sub>Q and is not to be used

$$Q_{2W} = \frac{Q_{2W} (1 + Q_{2W})}{Q_{2W} (1 + Q_{2W})} = 0.1$$



The angular resolution of the detecting system introduced errors in the counting rates at  $\Theta_N$  that are estimated to be less than three percent for all elements except lithium. In the case of lithium the error is estimated to be less than six percent. In calculating the results the finite resolution of the detecting system has been neglected. A more exact analysis should be made if a better theory is developed for the curve shapes. (See appendix I)

#### D. Reliability of the Data

The statistical spread in the data is large and is indicated on figures 6 through 11. As the process occurs more frequently in light nuclei (per gram of target) the counting rates were higher in the light nuclei and better statistics could be obtained. The statistical spread includes that associated with the subtraction of the accidental count. The accidental counting rate is an appreciable correction for the heavier elements especially at smaller neutron angles. In all elements except aluminum it seemed to be predictable on the basis of the resolving time of the equipment. In the case of aluminum the observed accidental rates were higher than the calculated values. When the aluminum data was corrected for the observed rate it was obvious that some failure had occurred in the circuit. For aluminum the calculated accidental rate as corroborated by the measurements on other elements was used.

The question of whether the curves go to zero at large angles from the center of the distribution or whether there is a constant

The angular resolution of the detecting system introduced errors in the counting rates of 6% that are estimated to be less than three percent for all elements except lithium. In the case of lithium the error is estimated to be less than six percent. In calculating the results the finite resolution of the detecting system has been neglected. A more exact analysis should be made if a better theory is developed for the curve shapes. (See Appendix I)

#### D. Reliability of the Data

The statistical spread in the data is large and is indicated on Figures 6 through 11. In the process counts were frequently in light nuclei (per gram of target) the counting rates were higher in the light nuclei and better statistics would be obtained. The statistical spread included that associated with the subtraction of the accidental count. The accidental counting rate is an appreciable correction for the heavier elements especially at smaller neutron energies. In all elements except lithium it seemed to be practicable on the basis of the resolving time of the equipment. In the case of lithium the observed accidental rates were higher than the calculated values. When the lithium data was corrected for the observed rate it was obvious that some lithium had occurred in the sample. For elements the calculated accidental rates as represented by the measurements on other elements was used.

The question of whether the curves go to zero at large angles

from the center of the distribution or whether there is a constant



(scattered) neutron background is very important in interpreting the results. For the light nuclei the curves were definitely observed to go to zero. However, in heavier nuclei (aluminum and copper) the accidental rate and poor statistics leave this question unresolved. Much longer runs and faster electronics circuitry than those employed would be needed to resolve this problem.

In that the ratios of  $\frac{N+P}{P}$  were used in obtaining the widths of curves, the measurements were self monitoring. Very conveniently such a ratio removes errors that would arise from fluctuations or drifts in the proton detecting system, the machine's intensity, and the machine's energy. The only drift or fluctuation not taken care of by this ratio are those arising in the neutron detecting system. Studies of the neutron detector by Christie<sup>31</sup> indicated that it was not a rapidly varying function of the bias where it was run. The mixing of the order of running the different angles of the neutron counter should have removed any systematic errors in the shape of the curve that would have arisen from instrumental errors.

Electronic failures were not sources of errors due to the double scalars on the important counting rates and the frequent checking of standards. In summary, the main sources of errors arising in the shapes of the curves are those associated with the accidental counting rates and counting statistics.

(accepted) neutron spectrum is very important in interpreting the results. For the light metal the curves were definitely observed to go to zero. However, in heavier metal (aluminum and copper) the additional rate and poor statistics lower this reaction markedly. Each larger rate and faster electronics directly show more analysis would be needed to resolve this problem.

In that the ratio of  $\frac{H}{L}$  was used in obtaining the values of curves, the measurements were well monitoring. Very conveniently such a ratio removes errors that would arise from fluctuations or drifts in the proton detecting system, the machine's intensity, and the machine's energy. The only drift or fluctuation not taken care of by this ratio are those arising in the neutron detecting system. Studies of the neutron detector by G. H. <sup>31</sup> indicated that it was not a rapidly varying function of the bias where it was run. The mixing of the order of turning the different angles of the neutron counter would have removed any systematic errors in the shape of the curve that would have arisen from instrumental errors.

Electronics failures were not sources of errors due to the double scales on the important counting rates and the frequent checking of standards.

In summary, the main sources of errors arising in the shape of the curves are those associated with the statistical counting rates and counting statistics.



## V. Results

### A. Deuterium

The angular distribution of neutrons in coincidence with protons from deuterium is shown in Figure 6 which plots the (subtracted) neutron-proton coincidences from deuterium normalized to the (subtracted) proton count of deuterium as the ordinate versus the angle of the neutron counter as the abscissa. These values are for a proton counter angle of  $76 \pm 5$  degrees and a proton energy of  $130 \pm 12$  Mev and are tabulated in the first and last columns of Table V. The deuterium curve is an experimental check on the angular and energy resolution of the telescopes as the deuteron in deuterium may be assumed at rest at the energies involved in this experiment. The full width at half height is 14 degrees which agrees with the value calculated from kinematics and the experimental arrangement<sup>31</sup>. This distribution went to zero on either side of its center.

### B. Lithium

The angular distribution of neutrons in coincidence with protons from lithium is shown in Figure 7 which plots the neutron-proton coincidences from lithium normalized to the proton count from lithium as the ordinate versus the angle of the neutron counter as the abscissa. These values are tabulated in the first and last columns of Table IV b. A broadening of the width at half height to 30 degrees is noted. Here a true angular spread in the neutron distribution is seen which is

## VI. Results

A. Deuterium

The angular distribution of neutrons in coincidence with protons from deuterium is shown in Figure 6 which plots the (unnormalized) neutron-proton coincidences from deuterium normalized to the (unnormalized) proton count of deuterium as the ordinate versus the angle of the neutron counter as the abscissa. These values are for a neutron counter angle of  $75 \pm 2$  degrees and a proton energy of  $150 \pm 12$  keV and are tabulated in the first and last columns of Table V. The deuterium curve is an experimental check on the angular and energy resolution of the telescopes as the deuterium in deuterium may be assumed at rest at the energies involved in this experiment. The full width at half height is 14 degrees which agrees with the value calculated from kinematics and the experimental arrangement.<sup>21</sup> This distribution was taken on either side of its center.

B. Lithium

The angular distribution of neutrons in coincidence with protons from lithium is shown in Figure 7 which plots the neutron-proton coincidences from lithium normalized to the proton count from lithium as the ordinate versus the angle of the neutron counter as the abscissa. These values are tabulated in the first and last columns of Table IV. A broadening of the width at half height to 30 degrees is noted. Here a true angular spread in the neutron distribution is seen which is

Figure 6

Neutron-Proton Coincidences from Deuterium

This is a plot of (subtracted) neutron-proton coincidences from deuterium normalized to the (subtracted) proton count from deuterium times  $10^3$  versus the angle of the neutron counter.



the first of these is the fact that the number of cases is small.

The second is the fact that the number of cases is small.

The third is the fact that the number of cases is small.

The fourth is the fact that the number of cases is small.

The fifth is the fact that the number of cases is small.

The sixth is the fact that the number of cases is small.

The seventh is the fact that the number of cases is small.

The eighth is the fact that the number of cases is small.

The ninth is the fact that the number of cases is small.

The tenth is the fact that the number of cases is small.

The eleventh is the fact that the number of cases is small.

The twelfth is the fact that the number of cases is small.

The thirteenth is the fact that the number of cases is small.

The fourteenth is the fact that the number of cases is small.

The fifteenth is the fact that the number of cases is small.

The sixteenth is the fact that the number of cases is small.

The seventeenth is the fact that the number of cases is small.

The eighteenth is the fact that the number of cases is small.

The nineteenth is the fact that the number of cases is small.

The twentieth is the fact that the number of cases is small.

The twenty-first is the fact that the number of cases is small.

The twenty-second is the fact that the number of cases is small.

The twenty-third is the fact that the number of cases is small.

The twenty-fourth is the fact that the number of cases is small.

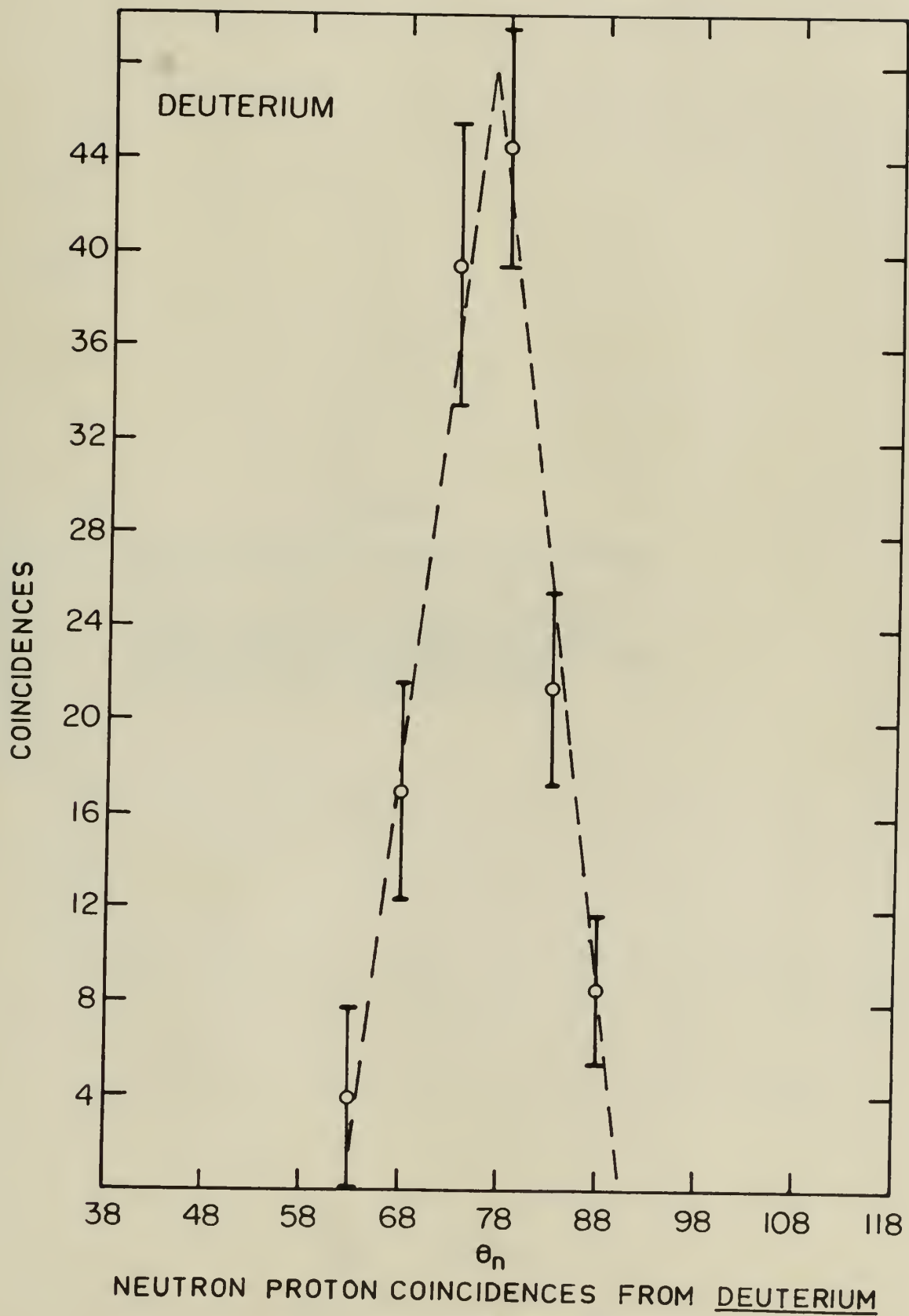


Figure 6





Figure 7

Neutron-Proton Coincidences from Lithium

This is a plot of neutron-proton coincidences from lithium normalized to the proton count from lithium times  $10^4$  versus the angle of the neutron counter.

## Figure 7

Neutron-Induced Fission of  $^{235}\text{U}$   
 This is a plot of neutron-induced fission  
 cross section versus neutron energy for  $^{235}\text{U}$ .  
 The curve shows the variation of the fission  
 cross section with neutron energy.

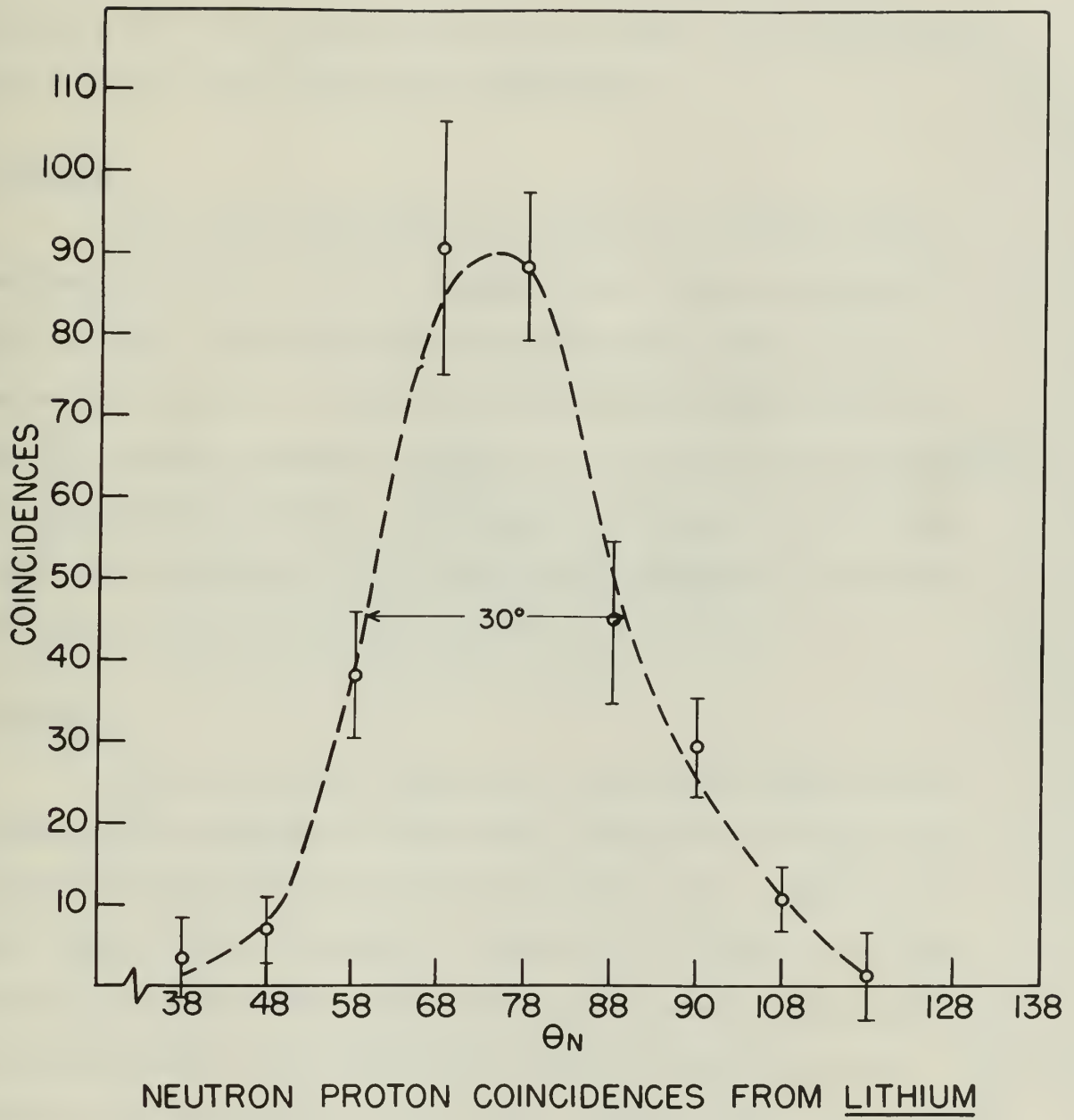


Figure 7





attributed to the presence of a finite momentum distribution within the nucleus for this type of experiment. This curve is in close agreement with that obtained by Barton and Smith<sup>31</sup>. The lithium curve went to zero on both sides of the distribution.

### C. Carbon

The angular distribution of neutrons in coincidence with protons from carbon is shown in Figure 8 which is the same type of plot as Figure 7 with the values obtained from the first and last columns of Table IVc. A further broadening of the half width to 41 degrees is noted indicating a greater spread in the momentum distribution over that found in lithium. Sufficient data was not taken at large angles from the center of the distribution to ascertain if the curve went to zero.

### D. Oxygen

Only the amount of light water data (hence oxygen data in neutron-proton scattering by gamma rays) required for the  $D_2O - H_2O$  subtraction for deuterium was taken during this work. However, the curve shown in Figure 9 which is a similar plot to Figure 7 was made up partly of data from previous work in this laboratory (published<sup>34</sup> and unpublished). The values plotted from this work are found in the first and last columns of Table IVd. Here the width at half height is 36 degrees which is not significantly different from that of carbon. The data has not been normalized in any way. This shows the reproducibility of such measurements over a period of six months. It should also

attributed to the presence of a finite momentum distribution within the nucleus for this type of experiment. This curve is in close agreement with that obtained by Barton and Smith<sup>31</sup>. The lithium curve went to zero on both sides of the distribution.

#### C. Carbon

The angular distribution of neutrons in coincidence with protons from carbon is shown in Figure 8 which is the same type of plot as Figure 7 with the values obtained from the first and last columns of Table IVc. A further broadening of the half width to 41 degrees is noted indicating a greater spread in the momentum distribution over that found in lithium. Sufficient data was not taken at large angles from the center of the distribution to ascertain if the curve went to zero.

#### D. Oxygen

Only the amount of light water data (neutron oxygen data in neutron-proton scattering by gamma rays) reported for the  $D_2O - H_2O$  subtraction for deuterium was taken during this work. However, the curve shown in Figure 9 which is a similar plot to Figure 7 was made up partly of data from previous work in this laboratory (published<sup>32</sup> and unpublished). The values plotted from this work are found in the first and last columns of Table IVd. Here the width of half width is 36 degrees which is not significantly different from that of carbon. The data has not been normalized in any way. This shows the unreliability of such measurements over a period of six months. It should also

Figure 8

Neutron-Proton Coincidences from Carbon

This is a plot of neutron-proton coincidences from carbon normalized to the proton count from carbon times  $10^4$  versus the angle of the neutron counter.

自 2007 年 1 月 1 日起

the ruins of the eastern country.  
 garden could have been there 10 years  
 hence from certain evidence in the  
 this is a plot of western-wooden cabin-  
 Western-wooden Colonization from 1840s



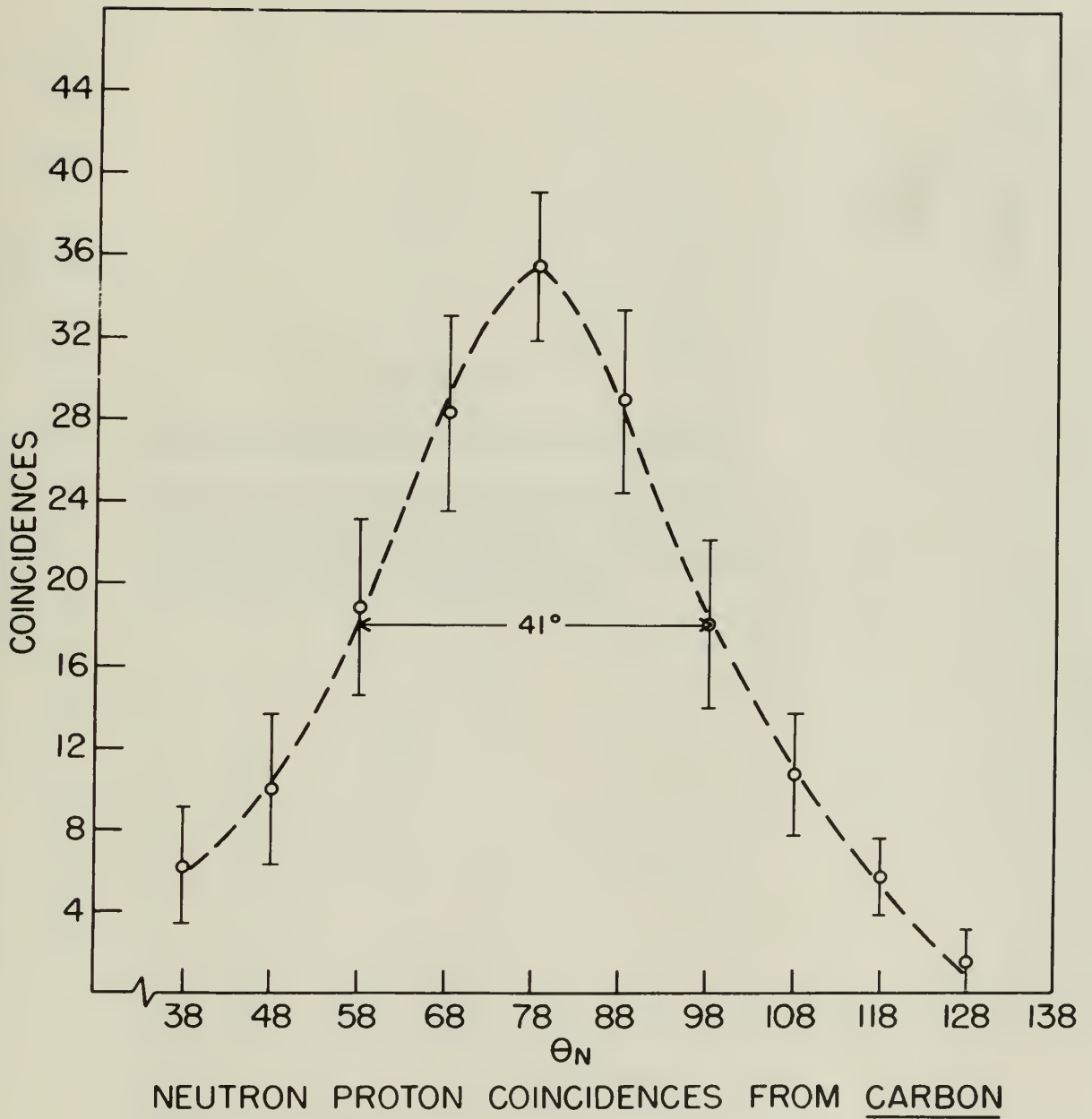


Figure 8



Figure 9

Neutron-Proton Coincidences from Oxygen

This is a plot of neutron-proton coincidences from oxygen normalized to the proton count from oxygen times  $10^4$  versus the angle of the neutron counter.

Figure 2

Neutron-Proton Coincidence from Oxygen  
 This is a plot of neutron-proton coinci-  
 dence from oxygen normalized to the  
 proton count from oxygen times 10<sup>4</sup> versus  
 the ratio of the neutron number.



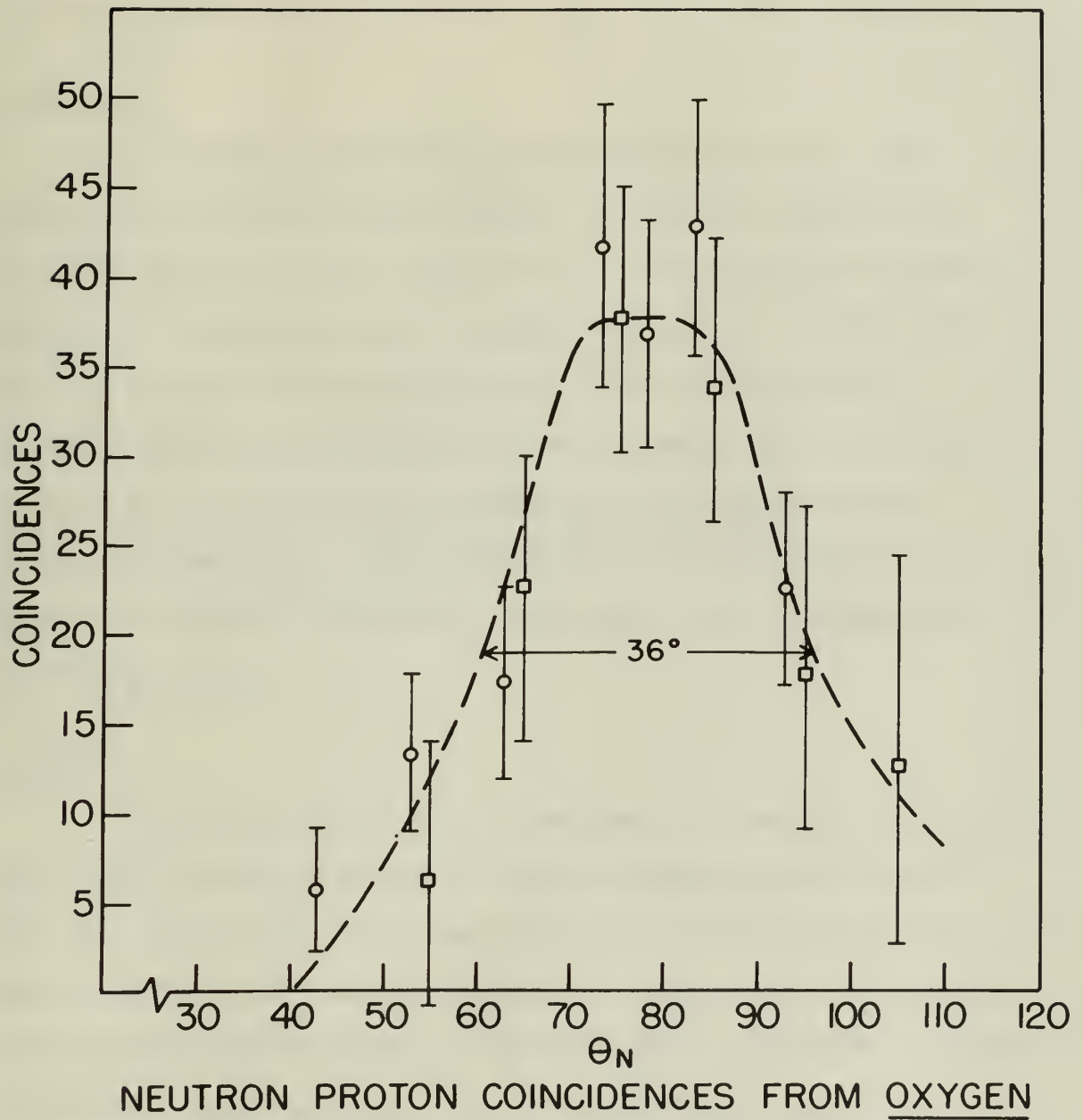


Figure 9



be noted that the statistical errors are larger than those in the other elements. The curve was carried to low enough angles to ascertain that it went to zero.

#### E. Aluminum

The angular distribution of neutrons in coincidence with protons from aluminum is shown in Figure 10 which is a similar plot to Figure 7 with the values obtained from the first and last columns of Table IVe. An apparent error\* was introduced into the aluminum data due to lowering the bias on the delayed neutron channel too far resulting in an erroneous accidental counting rate. This was corrected by using an average accidental counting rate based on the normal neutron counting rate as shown in Table IVe. Insufficient data was obtained to determine whether this curve went to zero on either side of the distribution.

#### F. Copper

The angular distribution of neutrons in coincidence with protons from copper is shown in Figure 11 which is a similar plot to Figure 7 with the values obtained from the first and last columns of Table IVf. Here the width at half height is 49 degrees which is not significantly different from that of aluminum. The statistical error in the data made it uncertain whether the curve goes to zero on either side of the distribution.

\*See Section IVC

be noted that the statistical errors are larger than those in the other elements. The curve was carried to low enough angles to ascertain that it went to zero.

#### E. Aluminum

The angular distribution of neutrons in coincidence with protons from aluminum is shown in Figure 10 which is a similar plot to Figure 7 with the values obtained from the first and last columns of Table IVe. An apparent error\* was introduced into the aluminum data due to lowering the bias on the delayed neutron channel too far resulting in an erroneous accidental counting rate. This was corrected by using an average accidental counting rate based on the normal neutron counting rate as shown in Table IVe. Insufficient data was obtained to determine whether this curve went to zero on either side of the distribution.

#### F. Copper

The angular distribution of neutrons in coincidence with protons from copper is shown in Figure 11 which is a similar plot to Figure 7 with the values obtained from the first and last columns of Table IVf. Here the width at half height is 49 degrees which is not significantly different from that of aluminum. The statistical error in the data made it uncertain whether the curve goes to zero on either side of the distribution.

\*See Section IVc



Figure 10

Neutron-Proton Coincidences from Aluminum

This is a plot of neutron-proton coincidences from aluminum normalized to the proton count from aluminum times  $10^4$  versus the angle of the neutron counter.

the first part of the 19th century, and the second part of the 19th century. The first part of the 19th century is the period of the first industrial revolution, and the second part of the 19th century is the period of the second industrial revolution.

## 1. Introduction

The second industrial revolution was a period of rapid technological change and economic growth. It was characterized by the development of new technologies, such as the steam engine, the telegraph, and the telephone. These technologies led to the growth of new industries, such as the railway, the telegraph, and the telephone. The second industrial revolution also led to the growth of the middle class and the rise of the nation-state. The second industrial revolution was a period of great change and growth, and it laid the foundation for the modern world.

## 2. The Second Industrial Revolution

The second industrial revolution was a period of rapid technological change and economic growth. It was characterized by the development of new technologies, such as the steam engine, the telegraph, and the telephone. These technologies led to the growth of new industries, such as the railway, the telegraph, and the telephone. The second industrial revolution also led to the growth of the middle class and the rise of the nation-state. The second industrial revolution was a period of great change and growth, and it laid the foundation for the modern world.

With respect to

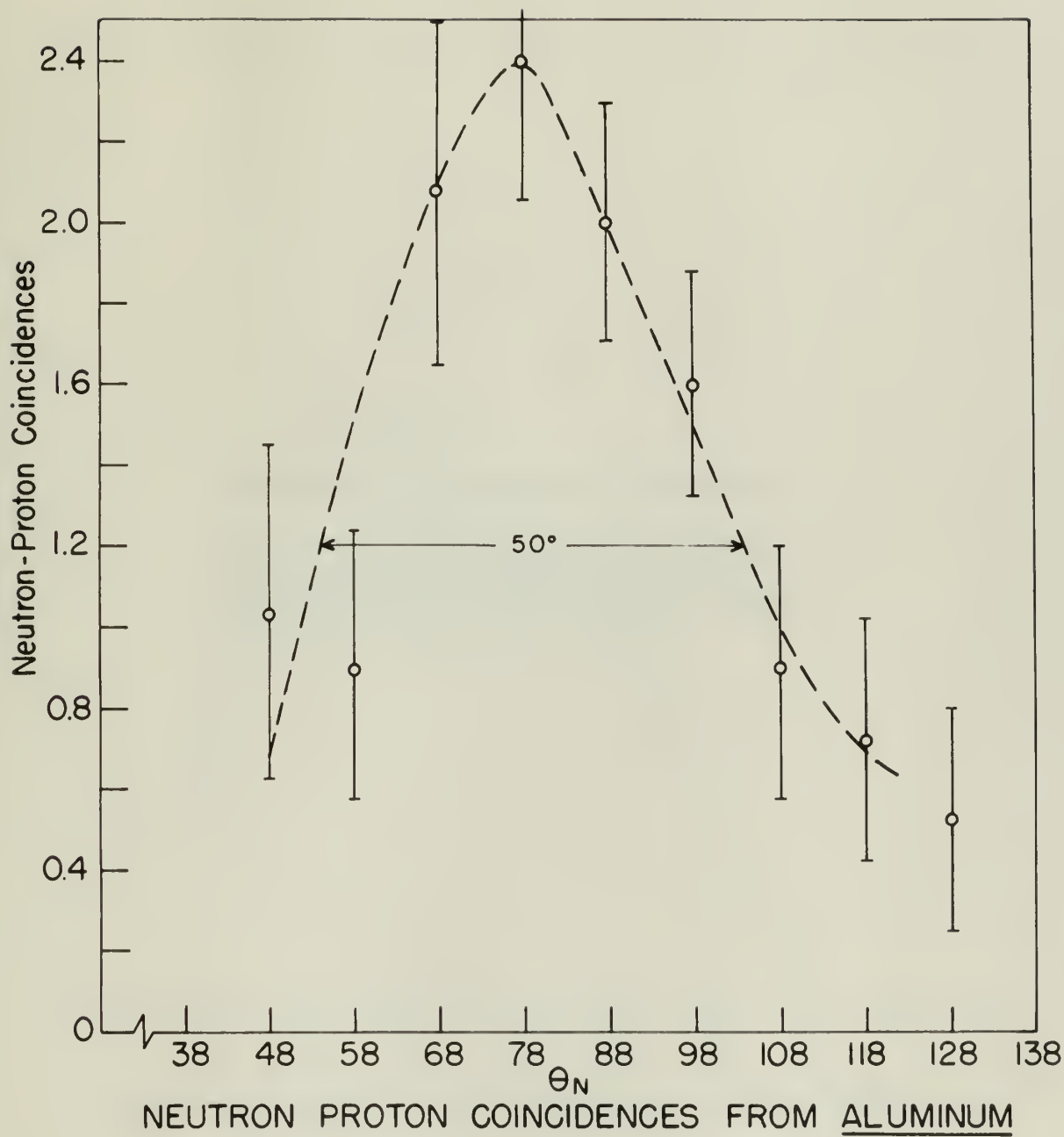


Figure 10





Figure 11

Neutron-Proton Coincidences from Copper

This is a plot of neutron-proton coincidences from copper normalized to the proton count from copper times  $10^4$  versus the angle of the neutron counter.

## Figure 11

Neutron-Proton Coincidence Time Spectrum  
 This is a plot of neutron-proton coincident  
 counts from a source normalized to the  
 proton count from a source  $10^4$  versus  
 the angle of the neutron counter.

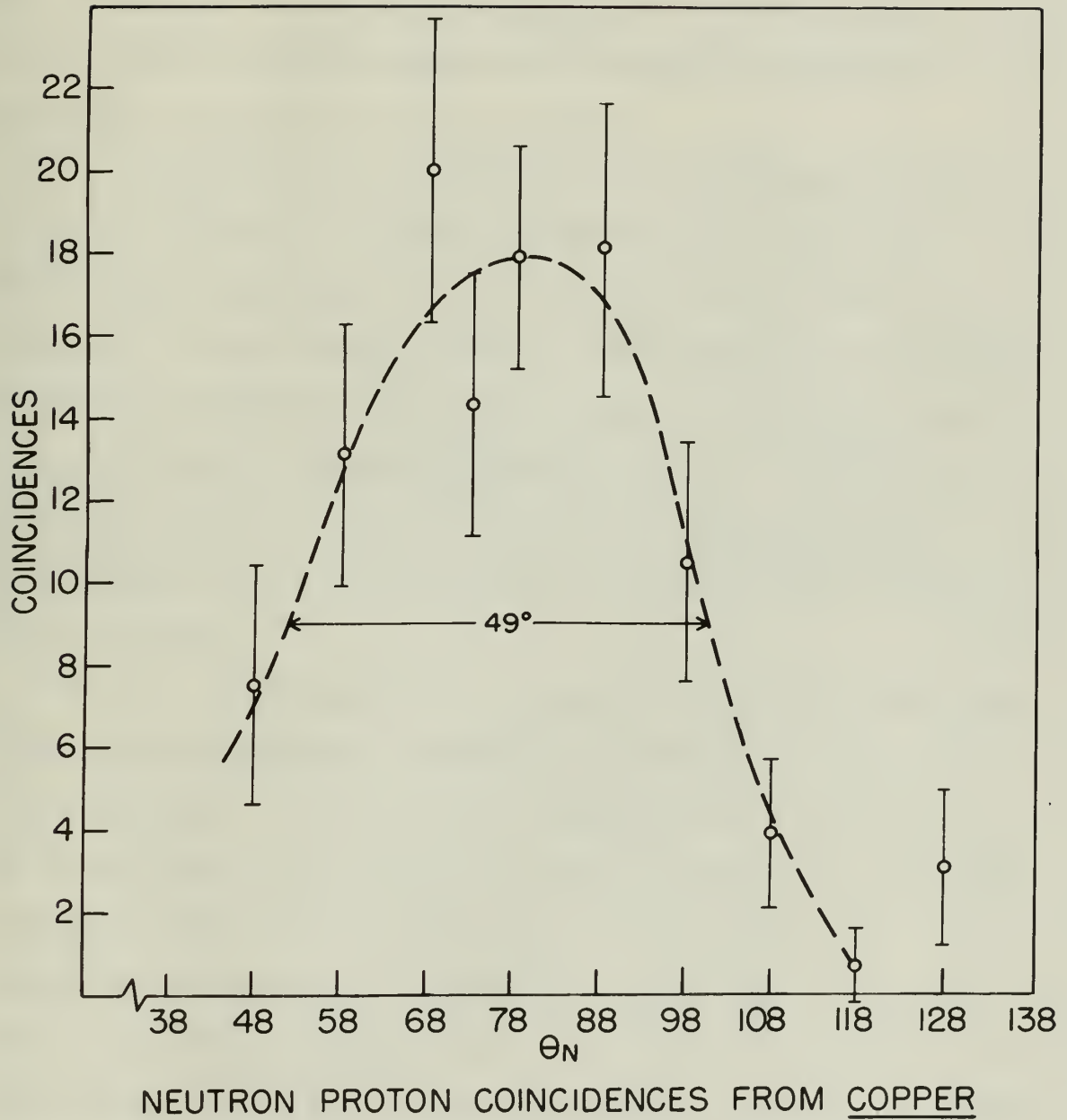


Figure 11





## VI. Conclusions

The purpose of this work was to employ the quasi-deuteron model of Levinger<sup>6</sup> as a mode of studying nuclear internal momenta. As an incidental result the quasi-deuteron model was substantially established with better data on more elements.

The detection of an angular spread in lithium beyond that due to the resolution of the detectors indicated the presence of a finite momentum distribution. A marked increase in the spread of the distribution occurred between lithium and carbon indicating an increase in the average momentum of the nucleons. However, the increase in the spread from carbon to aluminum and copper was slight. This does not necessarily indicate an increase in the average momentum since this slight increase could well be attributed to scattering of the neutrons within the nucleus.

A first approximation to a quantitative explanation of the shape of the angular distributions obtained has been derived by Wattenberg (see Appendix I). It is based on the assumptions that the nucleons in the nucleus have a three-dimensional gaussian momentum distribution, that neutrons and protons have the same momentum distributions, that it is possible to combine momenta and neglect the conservation of energy, and that the scattering of nucleons inside the nucleus can be neglected. The last assumption causes the calculated distribution to become less reliable with increasing atomic number as the effect of scattering becomes more pronounced with increasing nuclear dimensions.

## VI. Conclusions

The purpose of this work was to employ the quasi-deuteron model of Levinger<sup>6</sup> as a mode of studying nuclear internal structure. As an incidental result the quasi-deuteron model was substantially established with better data on more elements.

The detection of an angular spread in lithium beyond that

due to the resolution of the detectors indicated the presence of a finite momentum distribution. A marked increase in the spread of the distribution occurred between lithium and carbon indicating an increase in the average momentum of the nucleons. However, the increase in the spread from carbon to aluminum and copper was slight. This does not necessarily indicate an increase in the average momentum since this slight increase could well be attributed to scattering of the nucleons within the nucleus.

A first approximation to a quantitative estimation of the shape

of the angular distribution obtained is now derived by following (see Appendix I). It is based on the assumption that the nucleons in the nucleus have a three-dimensional Gaussian momentum distribution, that neutrons and protons have the same momentum distribution, that it is possible to combine momenta and neglect the conservation of energy, and that the scattering of nucleons inside the nucleus can be neglected. The last assumption causes the calculated distribution to become less reliable with increasing atomic number as the effect of scattering becomes more pronounced with increasing nuclear dimensions.



With the above assumptions and neglecting the finite resolution of the detectors the curve would have a distribution about the midpoint given by

$$N(\psi) \sin \psi d\psi = N_0 e^{-\frac{\sin^2 \psi}{\sin^2 \psi_0} \left( \frac{\sin^2 \psi_0}{2} + \cos^2 \psi \right) \sin \psi d\psi}$$

where  $\psi$  is the angle from the midpoint of the distribution (78 degrees) and  $\sin^2 \psi_0 = \frac{2E_g}{E_p}$  where  $E_p$  is the energy of the proton in the laboratory and  $E_g$  is the 1/e value of the initial gaussian distribution of the momenta of the nucleons in the nucleus. The term  $\frac{\sin^2 \psi_0}{2}$  can generally be neglected as being of the order of 0.1

Figure 12 shows a semilogarithmic plot of  $\frac{\text{coincidences}}{\cos^2 \psi}$  vs  $\sin^2 \psi$  which should give a straight line on semilogarithmic paper within the accuracy of the experiment and the theory. Only lithium, carbon and oxygen are shown as the heavier elements possessed a rise in  $\frac{\text{coincidences}}{\cos^2 \psi}$  at larger  $\psi$ . The rise at large  $\psi$  in the heavier elements can be attributed to the incidence of scattering in the heavier nuclei. The values of  $E_g$  as obtained from the plot are  $9 \pm 1.5$  Mev for lithium,  $19 \pm 1.5$  Mev for carbon and approximately 19 Mev for oxygen. The oxygen plot suffers from being the result of two different collimations of the proton counter and in not being normalized. The uncertainty of  $\pm 1.5$  Mev on the lithium and carbon results were obtained from the extreme slopes which could be fitted to the data. It should be noted that the 1/e values obtained for these two elements are much more definitely fixed by this experiment than in previous works. However, the values obtained are in the neighborhood of those previously obtained for other

the above assumptions and neglecting the finite resolution

of the detector the curve would have a distribution about the midpoint

given by

$$W(\psi) \sin \psi \frac{1}{2} \psi = W_0 \left( \frac{\sin \frac{1}{2} \psi}{\frac{1}{2} \psi} + \cos \psi \right) \sin \frac{1}{2} \psi$$

where  $\psi$  is the angle from the midpoint of the distribution (78 degrees) and  $\sin \psi = \frac{2E_0}{E}$  where  $E_0$  is the energy of the proton in the laboratory

and  $E_0$  is the value of the initial meson distribution of the moments of the nucleus in the nucleus. The term  $\frac{\sin \frac{1}{2} \psi}{\frac{1}{2} \psi}$  can generally

be neglected as being of the order of 0.1

Figure 12 shows a semi-logarithmic plot of  $\frac{\cos \psi}{\cos \frac{1}{2} \psi}$

as  $\sin \frac{1}{2} \psi$  which should give a straight line on semi-logarithmic paper within the accuracy of the experiment and the theory. Only lithium, carbon and

oxygen are shown as the heavier elements possessed a rise in  $\frac{\cos \psi}{\cos \frac{1}{2} \psi}$

at larger  $\psi$ . The rise at large  $\psi$  in the heavier elements can be

attributed to the incidence of scattering in the heavier nuclei. The

values of  $E_0$  are obtained from the plot are 9, 1.5 Mev for lithium,

19, 1.5 Mev for carbon and approximately 19 Mev for oxygen. The oxygen

plot suffers from being the result of two different calculations of the

proton counter and is not being normalized. The uncertainty of  $\pm 1.5$

Mev on the lithium and carbon results were obtained from the extreme

slopes which could be fitted to the data. It should be noted that the

1/e values obtained for these two elements are much more definitely

fixed by this experiment than in previous works. However, the values

obtained are in the neighborhood of those previously obtained for other



Figure 12

Fit of Experimental Data for Lithium, Carbon and Oxygen to Theoretical  
Curve Shape

This is a plot of  $\frac{\text{coincidences}}{\cos^2 \psi}$  versus  $\sin^2 \psi$  which should be a straight  
line within the errors of the experiment if the experimental results  
fit the theory.

The first of these is the fact that the rate of reaction is independent of the concentration of the reactants. This is a characteristic feature of a zero-order reaction.

The second feature is that the rate of reaction decreases linearly with time. This is also a characteristic feature of a zero-order reaction.

The third feature is that the reaction eventually comes to a stop. This is also a characteristic feature of a zero-order reaction.

Figure 12 shows the rate of reaction as a function of time. The rate decreases linearly from its initial value to zero.

This is a plot of  $\ln \frac{a-x}{a}$  versus time. The plot is a straight line, which is characteristic of a first-order reaction.

The slope of the line is equal to the rate constant,  $k$ . This is a characteristic feature of a first-order reaction.

The intercept of the line on the y-axis is equal to  $\ln a$ . This is also a characteristic feature of a first-order reaction.

The half-life of the reaction is equal to  $\frac{\ln 2}{k}$ . This is a characteristic feature of a first-order reaction.

The rate of reaction is proportional to the concentration of the reactant. This is a characteristic feature of a first-order reaction.

The reaction is first-order with respect to the reactant. This is a characteristic feature of a first-order reaction.

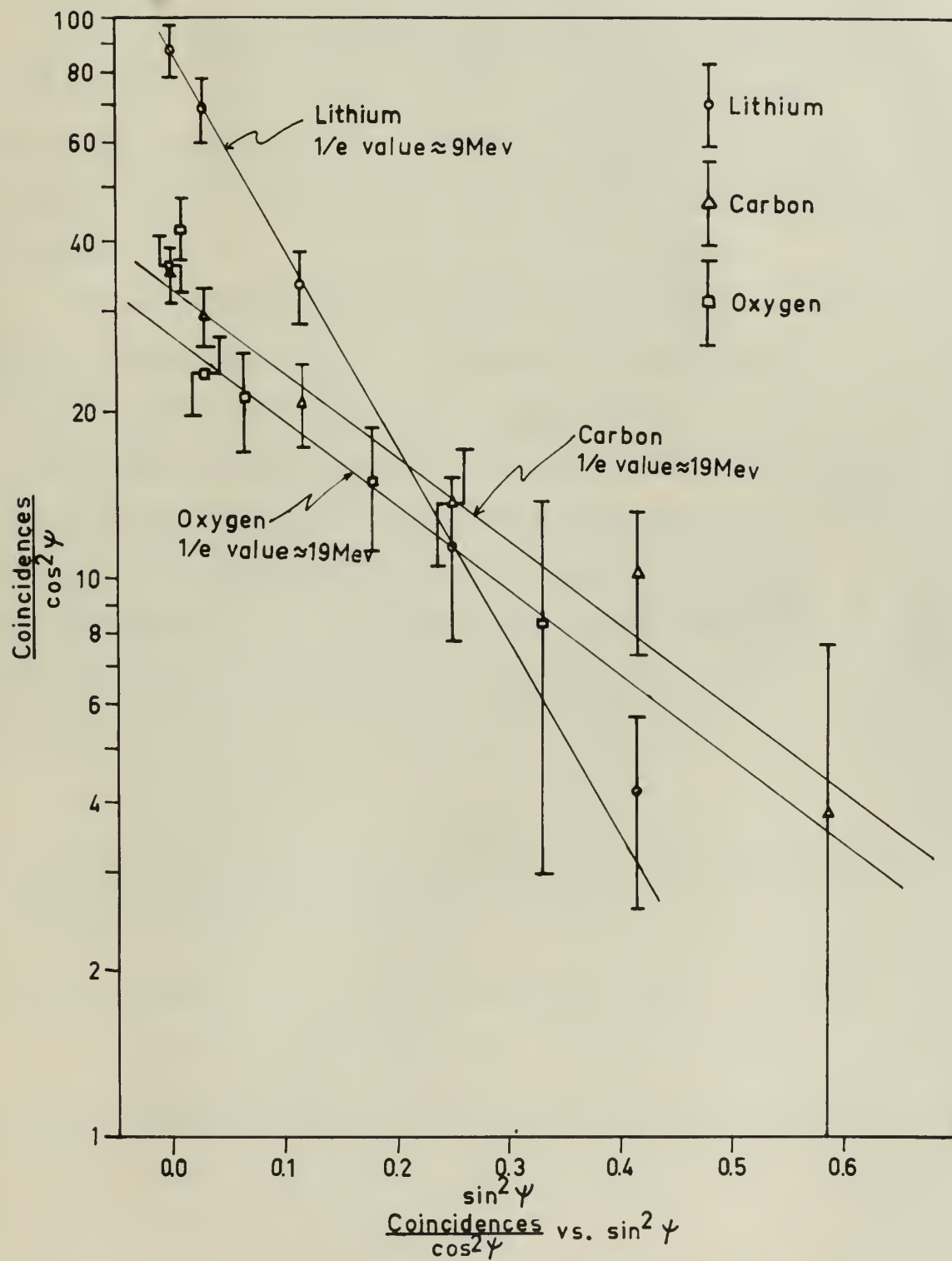


Figure 12





light elements<sup>22</sup>.

The reason for the apparent rise in the carbon and oxygen curves for small  $\psi$  is not clear. If it is not due to experimental causes, and if a more exact theory of the curve shapes should leave it unexplained, then the possibility exists that it is caused by nuclear shell effects.

Future work should undertake the examination of more nuclei (especially the heavier ones) and the extension of the observations over wider angles from the center of the distributions. With data from observations at larger angles from the midpoint of the distribution it may be possible to subtract off the scattered neutron background and hence obtain curves which may better fit the theory of Appendix I. Modification and improvement of the theory to include such effects as the scattered neutron background should be attempted.

light element.

The reason for the statement is in the neutron and oxygen

curves for small  $\psi$  is not clear. If it is not due to experimental

errors, and if a more exact theory of the curve shapes should have

it would be, then the possibility exists that it is caused by nuclear

shell effects.

There are also some indications of some small

(especially the heavier ones) and the extension of the observations

over other angles from the nature of the distribution. With data

from observations at larger angles from the midpoint of the distribution

it may be possible to extend all the neutron distribution and

these other curves will be better fit the theory of Appendix I.

Qualitative and quantitative of the theory in relation with others as

the neutron neutron background should be extended.

## BIBLIOGRAPHY

1. For a summary of work up to 1952 see K. Strauch, *Ann. Rev. Nuclear Sci.* 2, 105 (1953)
2. B. T. Feld, R. D. Godbole, A. Odian, F. Scherb, P. C. Stein and A. Wattenberg, *Phys. Rev.* 94, 1000 (1954). See this paper for references to other work.
3. C. Levinthal and A. Silverman, *Phys. Rev.* 82, 822 (1951)
4. D. Walker, *Phys. Rev.* 81, 634 (1951); 84, 149 (1951)
5. J. C. Keck, *Phys. Rev.* 85, 410 (1952)
6. J. S. Levinger, *Phys. Rev.* 84, 43 (1951)
7. J. W. Rosengren and J. M. Dudley, *Phys. Rev.* 89, 603 (1953)
8. A. M. Perry and J. C. Keck, *Phys. Rev.* 86, 629 (1952)
9. J. W. Weil and B. D. McDaniel, *Phys. Rev.* 92, 391 (1953)
10. T. S. Benedict and W. M. Woodward, *Phys. Rev.* 85, 924 (1952)
11. W. S. Gilbert and J. W. Rosengren, *Phys. Rev.* 88, 901 (1952)
12. H. Myers, A. Odian, P. C. Stein and A. Wattenberg, *Phys. Rev.* 95, 576 (1954)
13. M. Q. Barton and J. H. Smith, *Phys. Rev.* 95, 573 (1954)
14. M. Wiener, Energy and Angle Distribution of the Photoprotons from Deuterium, National Bureau of Standards Circular 515, U. S. Government Printing Office (1951)
15. E. Fermi, Jay Orear, A. H. Rosenfeld and R. A. Schluter, Nuclear Physics, University of Chicago Press, 1950, p. 159
16. G. F. Chew and M. L. Goldberger, *Phys. Rev.* 77, 470 (1950)
17. For a discussion of nuclear radii see R. D. Evans, The Atomic Nucleus, McGraw-Hill Book Co. Inc. (1955) Chapter II
18. J. Hadley and H. F. York, *Phys. Rev.* 80, 345 (1950)
19. J. Heidman, *Phys. Rev.* 80, 171 (1950)
20. O. Chamberlain and E. Segrè, *Phys. Rev.* 87, 81 (1952)



## BIBLIOGRAPHY

1. For a summary of work up to 1951 see E. G. Lomonosov, *Ann. Rev. Phys. Chem.* **21**, 105 (1951).
2. E. T. Bell, E. D. Collip, A. Collins, V. Schor, P. E. Klein and A. Weissberger, *Phys. Rev.* **100** (1954). See this paper for references to other work.
3. T. Lashfield and A. G. Lomonosov, *Phys. Rev.* **82**, 625 (1951).
4. D. Weiser, *Phys. Rev.* **81**, 624 (1951); **81**, 149 (1951).
5. L. C. Koss, *Phys. Rev.* **82**, 410 (1952).
6. J. G. Lashfield, *Phys. Rev.* **81**, 43 (1951).
7. J. H. Lomonosov and J. W. Lashfield, *Phys. Rev.* **81**, 601 (1953).
8. A. M. Potts and L. C. Koss, *Phys. Rev.* **80**, 629 (1950).
9. J. W. Lashfield and B. G. Lomonosov, *Phys. Rev.* **92**, 391 (1953).
10. T. L. Lashfield and E. V. Lashfield, *Phys. Rev.* **81**, 624 (1951).
11. E. G. Lashfield and A. G. Lomonosov, *Phys. Rev.* **81**, 601 (1953).
12. H. Lashfield, A. Collins, E. G. Lashfield and A. Weissberger, *Phys. Rev.* **92**, 276 (1954).
13. M. G. Lashfield and E. G. Lashfield, *Phys. Rev.* **92**, 273 (1954).
14. E. Lashfield, *Report and Analysis of the Distribution of the Spectroscopic Data*, National Bureau of Standards Circular 505, U. S. Government Printing Office (1951).
15. E. Lashfield, J. G. Lashfield and E. G. Lashfield, *Phys. Rev.* **92**, 276 (1954).
16. E. Lashfield and E. G. Lashfield, *Phys. Rev.* **92**, 273 (1954).
17. For a discussion of nuclear radii see E. T. Bell, *The Atomic Nucleus*, McGraw-Hill Book Co. Inc. (1955) Chapter II.
18. L. Lashfield and E. G. Lashfield, *Phys. Rev.* **90**, 345 (1950).
19. J. Lashfield, *Phys. Rev.* **90**, 171 (1950).
20. C. Lashfield and E. G. Lashfield, *Phys. Rev.* **81**, 624 (1951).



21. J. B. Cladis (Thesis), University of California Radiation Laboratory Report No. 1621 and J. B. Cladis, W. N. Hess and B. J. Moyer, Phys. Rev. 87, 425 (1952)
22. J. M. Wilcox (Thesis), University of California Radiation Laboratory Report No. 2540 (1954)
23. W. G. McMillan and E. Teller, Phys. Rev. 72, 1 (1947)
24. E. Henley and R. Huddleston, Phys. Rev. 82, 754 (1951)
25. E. M. Henley, Phys. Rev. 85, 204 (1952)
26. M. M. Block, S. Passman and W. W. Havens, Phys. Rev. 83, 167 (1951)
27. M. M. Block, S. Passman and W. W. Havens, Phys. Rev. 88, 1239 (1952)
28. R. Bjorklund, W. E. Crandall, B. J. Moyer and H. F. York, Phys. Rev. 77, 213 (1950)
29. J. Steinberger and A. S. Bishop, Phys. Rev. 78, 494 (1950)
30. M. Lax and H. Feshback, Phys. Rev. 81, 189 (1951)
31. E. R. Christie (Thesis) M.I.T., Unpublished (1955)
32. A. C. Odian (Thesis) M.I.T., Unpublished (1955)
33. H. C. Ratz (Thesis) M.I.T., Unpublished (1952)
34. A. C. Odian, W. A. Rankin, P. C. Stein and A. Wattenberg, M.I.T. Laboratory for Nuclear Science Progress Report November 30, 1954, Page 30

21. J. B. CLARK (Thesis), University of California Radiation Laboratory Report No. 1421 and J. B. CLARK, W. H. HARRIS and J. J. HARRIS, *Phys. Rev.* **82**, 455 (1952)
22. J. V. ALLEN (Thesis), University of California Radiation Laboratory Report No. 1420 (1952)
23. W. C. WENDLIN and R. J. JELINEK, *Phys. Rev.* **85**, 1 (1952)
24. R. WELBY and W. WENDLIN, *Phys. Rev.* **85**, 754 (1952)
25. R. WELBY, *Phys. Rev.* **85**, 204 (1952)
26. R. WELBY, R. F. FARMAN and J. H. HARRIS, *Phys. Rev.* **85**, 147 (1952)
27. R. H. BLOCH, R. FARMAN and J. H. HARRIS, *Phys. Rev.* **85**, 147 (1952)
28. R. WELBY, R. F. FARMAN, R. J. JELINEK and J. V. ALLEN, *Phys. Rev.* **85**, 147 (1952)
29. J. WELBY and R. J. JELINEK, *Phys. Rev.* **85**, 147 (1952)
30. R. WELBY and R. J. JELINEK, *Phys. Rev.* **85**, 147 (1952)
31. J. WELBY (Thesis), M.I.T., unpublished (1952)
32. J. WELBY (Thesis), M.I.T., unpublished (1952)
33. J. WELBY (Thesis), M.I.T., unpublished (1952)
34. J. WELBY, R. J. JELINEK, J. V. ALLEN and J. H. HARRIS, *Phys. Rev.* **85**, 147 (1952)

## Appendix I

# A Crude Theory of the Neutron-Proton Coincidence Curve Shapes

(Developed by Dr. A. Wattenberg)

Assume momentum is that of a ground state of an harmonic oscillator potential; then, for the proton

$$\phi(p) = N e^{-\frac{p_x^2 + p_y^2 + p_z^2}{2p_0^2}}$$

where N is a normalizing constant

The density in momentum space is

$$\phi^*(p) \phi(p) dp_x dp_y dp_z = N^2 e^{-\frac{p_x^2 + p_y^2 + p_z^2}{p_0^2}} dp_x dp_y dp_z \quad (1)$$

Similarly for the neutron momentum density

$$\phi^*(q) \phi(q) dq_x dq_y dq_z = N^2 e^{-\frac{q_x^2 + q_y^2 + q_z^2}{q_0^2}} dq_x dq_y dq_z$$

The momentum density of the pair of particles is

$$N^4 e^{-\frac{p_x^2 + q_x^2 + p_y^2 + q_y^2 + p_z^2 + q_z^2}{p_0^2}} dp_x dq_x dp_y dq_y dp_z dq_z \quad (2)$$

assuming  $p_0 = q_0$

Let	$\vec{P} = \vec{p} + \vec{q}$	$\vec{Q} = \vec{p} - \vec{q}$
	$P_x = p_x + q_x$	$Q_x = p_x - q_x$
	$P_y = p_y + q_y$	$Q_y = p_y - q_y$
	$P_z = p_z + q_z$	$Q_z = p_z - q_z$
	$p_x = \frac{P_x + Q_x}{2}$	$q_x = \frac{P_x - Q_x}{2}$

Then

$$P_x^2 + Q_x^2 = p_x^2 + 2p_x q_x + q_x^2 + p_x^2 - 2p_x q_x + q_x^2 = 2p_x^2 + 2q_x^2$$

Or

$$p_x^2 + q_x^2 = \frac{P_x^2 + Q_x^2}{2}$$





$$dP_x dQ_x = J \left( \frac{P_x, Q_x}{P_x, Q_x} \right) dP_x dQ_x$$

$$J_x = \left| \left( \frac{\partial P_x}{\partial P_x} \right) \left( \frac{\partial Q_x}{\partial Q_x} \right) - \left( \frac{\partial P_x}{\partial Q_x} \right) \left( \frac{\partial Q_x}{\partial P_x} \right) \right|$$

$$= \left| \left( \frac{1}{2} \right) \left( -\frac{1}{2} \right) - \left( \frac{1}{2} \right) \left( \frac{1}{2} \right) \right| = \frac{1}{2}$$

Thus (2) becomes

$$N^4 e^{-\frac{P_x^2 + Q_x^2 + P_y^2 + Q_y^2 + P_z^2 + Q_z^2}{2P_0^2}} J_x J_y J_z dP_x dP_y dP_z dQ_x dQ_y dQ_z$$

or  $N^4 e^{-\frac{P_x^2 + P_y^2 + P_z^2}{P_0^2}} dP_x dP_y dP_z \times \frac{1}{8} \times \iiint_{-\infty}^{\infty} e^{-\frac{Q_x^2 + Q_y^2 + Q_z^2}{P_0^2}} dQ_x dQ_y dQ_z$

$$P_0 = 1.4 p_0$$

$$\text{or } \left[ \frac{N^4 P_0^3 \pi^{3/2}}{8} \right] e^{-\frac{P_x^2 + P_y^2 + P_z^2}{P_0^2}} dP_x dP_y dP_z \quad (3)$$

#### APPROXIMATE THREE-DIMENSIONAL CASE

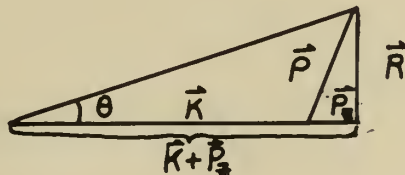
Use cylindrical coordinates

Let  $R^2 = P_x^2 + P_y^2$

$$\iint dP_x dP_y = \int_0^{2\pi} \int_0^{\infty} R dR d\theta$$

$$P^2 = R^2 + P_z^2$$

$$\tan \theta = \frac{R}{K + P_z} \quad 0 < \theta < \frac{\pi}{2}$$



Approximations

$$\theta \ll 1 \quad K \gg P_z \quad \text{then } R = K\theta$$



(3) becomes

$$e^{-\frac{R^2}{P_0^2}} 2\pi R dR e^{-\frac{P_z^2}{P_0^2}} dP_z \quad (4)$$

$$R dR = K^2 \theta d\theta$$

and (4) becomes

$$2\pi K^2 e^{-\frac{K^2 \theta^2}{P_0^2}} \theta d\theta \int_{-\infty}^{\infty} e^{-\frac{P_z^2}{P_0^2}} dP_z$$

$$\text{or } 2\pi K^2 P_0 \sqrt{\pi} e^{-\frac{K_0^2}{P_0^2} \theta^2} \theta d\theta$$

Hence, the approximate three-dimensional curve shape is

$$e^{-\frac{K^2}{P_0^2} \theta^2} \theta d\theta \quad 0 < \theta < \frac{\pi}{2}$$

An exact three-dimensional curve shape has been derived in the following form:

$$2\pi^{3/2} P_0 \left[ \frac{P_0^2}{2} + K^2 \cos^2 \theta \right] \sin \theta e^{-\frac{K^2}{P_0^2} \sin^2 \theta} d\theta$$

$$0 < \theta < \frac{\pi}{2}$$















Theory  
636

28993

Wilson

High energy photo-  
ejection of neutron-  
proton pairs from various  
nuclei.

Theory  
636

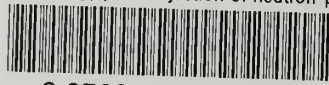
28993

Wilson

High energy photo-ejection  
of neutron-proton pairs from  
various nuclei.

thesW636

High energy photo-ejection of neutron-pr



3 2768 001 90132 5

DUDLEY KNOX LIBRARY